How High Can You Go: Determining the warmest supply water temperature for high thermal mass radiant cooling systems under thermal comfort constraints

Carlos Duarte Roa[1], Paul Raftery[1], Stefano Schiavon[1], Fred Bauman[1]
[1]*Center for the Built Environment, University of California, Berkeley, CA, USA*

Highlights

- High thermal mass radiant systems (HTMR) should use high-temperature cooling.
- Design supply water temperatures of ≥18.2 °C were possible in 50% of the test cases.
- Building designers should use 24-hour mean heat gains instead of peak heat gains to size HTMR.
- 21/30 climates tested allows ≥40% waterside economizer operation with 4 °C approach temperature.
- HTMR systems reduce capital and operational cooling costs in all US climates.

Keywords

High thermal mass radiant systems, Evaporative cooling, Low energy cooling, Energy simulation, High-performance buildings

https://doi.org/10.1016/j.enbuild.2025.115387
escholarship.org/uc/item/3812p9p1

Abstract

The need for cooling in buildings is mainly handled using systems based on the refrigeration cycle, often an energy- and cost-intensive process. High thermal mass radiant systems (HTMR) enable the use of warmer than typical chilled water temperatures to provide cooling. In favorable weather conditions, the cooled water can be produced through low-energy and low-cost cooling devices. In this two-phased study, we first determined the warmest supply water temperature (SWT) needed in HTMR that maintains thermally comfortable conditions on the cooling design day. Then, we investigated the potential of replacing the refrigeration cycle with evaporative cooling devices in the primary cooling system. We performed a quasi-random sampling of building and HTMR system design parameters representing typical building characteristics and design cooling loads for lighting, people, and plug loads to create 360,900 single zone EnergyPlus models. We iteratively simulated the models on the climate zones' cooling design day to find the warmest SWT that did not exceed a maximum zone operative temperature of 26 °C. The test cases include simulations using 14 ASHRAE and 16 California climate zones. The results show that HTMR can use SWT of 12.3, 18.2, and 21.1 °C for the 25th, 50th, and 75th percentile, respectively, of test cases, indicating that overall cooling energy and costs can be reduced in all US climates through high-temperature cooling. In addition, high-temperature cooling allows at least 40% of waterside economizer operation during the cooling season for 21 out of 30 climate zones with reasonably performing evaporative cooling devices.

https://doi.org/10.1016/j.enbuild.2025.115387
escholarship.org/uc/item/3812p9p1

Graphical Abstract

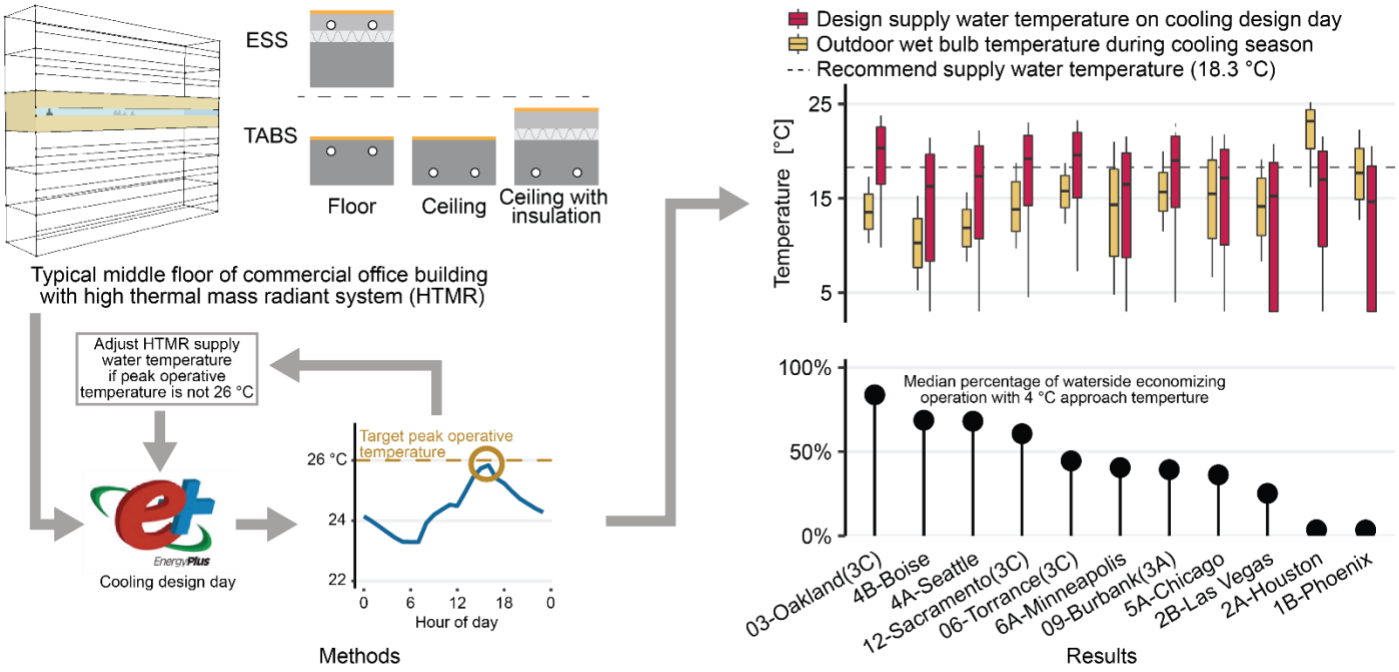

https://doi.org/10.1016/j.enbuild.2025.115387
escholarship.org/uc/item/3812p9p1

List of symbols

kg_w Kilograms of water vapor [kg]
kg_{da} Kilograms of dry air [kg]
$\dot{V}_{tlt}$ Total volumetric flow rate [$m^3 \cdot s^{-1}$]
$\hat{\dot{V}}_{area}$ Volumetric water flow rate per floor area [$l \cdot s^{-1} \cdot m^{-2}$]
$HG_{sim_{zn}}^{sen}$ Simulated sensible heat gain energy introduced into the zone [kWh]
$\overline{HG}_{\Delta T}$ 24-hour mean sensible heat gains divided by the design supply/return temperature difference [$W \cdot m^{-2} \cdot K^{-1}$]
ΔR_{X-G} Difference between design hydronic extraction energy in 24-hours and simulated heat gain energy [-]
Δt_{hyd} Number of operation hours in HTMR [h]
ΔT_{r-s} Design supply/return temperature difference [K]
Q_{hyd} Design hydronic extraction energy in 24-hours [kWh]
q_{ISO} ISO 11855-2012 design capacity [$W \cdot m^{-2}$]
c_p Fluid specific heat [$J \cdot kg^{-1} \cdot K^{-1}$]
ρ Fluid density [$kg \cdot m^{-3}$]
ε Error between SWT and maximum operative temperature during occupied hours [°C]
η Tolerance for stopping iteration of finding SWT [°C]

https://doi.org/10.1016/j.enbuild.2025.115387
escholarship.org/uc/item/3812p9p1

1. Introduction

The need for cooling is a significant driver of energy consumption in buildings and is mainly handled using heating, ventilation, and air conditioning (HVAC) systems based on the refrigeration cycle, which is energy- and cost-intensive. In the US, HVAC accounts for 51.3% of the total site energy consumed in commercial buildings; 31.9%, 8.7%, 10.7% for space heating, cooling, and ventilation, respectively (EIA 2022). Most HVAC site energy consumption currently goes to heating, but shifts in economic and population growth, building design and use, adoption rates to efficient heating equipment such as heat pumps, and climate change are expected to decrease heating and increase cooling needs in the US and on a global scale (Isaac and van Vuuren 2009; Zhou, Eom, and Clarke 2013; Zhou et al. 2014; Dean et al. 2018).

High-temperature cooling, i.e. using higher than typical supply water temperature (SWT) to perform space cooling, is a potential design strategy to avoid increases in space cooling energy while providing thermal comfort. Commercial building chilled water plants are typically designed to supply water at 5.6-7.2 °C to variable or constant air zone terminal units to maintain the desired zone setpoint temperature (Taylor 2011). Increasing the leaving chilled water temperature while maintaining the same condenser water system, increases the chiller's compressor efficiency (Seshadri, Rysanek, and Schlueter 2019). One way to achieve high-temperature cooling is through a decoupled system where separate HVAC components extract the building's sensible and latent loads. The literature shows that chilled beams and radiant systems with separate ventilation systems (usually a dedicated outdoor air system (DOAS)) are the favored HVAC system topology to achieve high-temperature cooling (Saber, Tham, and Leibundgut 2016; Seshadri, Rysanek, and Schlueter 2019). In a building in a tropical climate, a radiant system showed up to 34% measured energy savings compared to an all-air system (Li et al. 2024).

In this study, we focus on radiant systems with DOAS. Specifically, we focus on radiant systems with a large quantity of inherent thermal mass, as described below. Radiant systems are an HVAC system that delivers 50% or more of the design heat transfer to occupants through thermal radiation (ASHRAE 2020). Karmann et al.'s (2017b) results indicate that "radiant and all-air spaces have equal indoor environmental quality, including acoustic satisfaction, with a tendency towards improved temperature satisfaction in radiant buildings" (Karmann, Schiavon, and Bauman 2017; Karmann et al. 2017). They are also a significant component that facilitates net-zero buildings (Higgins and Carbonnier 2017). Radiant systems come in different variations, but there is no clear consensus on a formal definition for them. International standards and guidelines currently classify radiant systems based on their structure and geometry. The three main types are embedded surface systems (ESS), thermally activated building systems (TABS), and radiant ceiling panels (RCP). A drawback to classifying radiant systems based on their structure and geometry is that it fails to provide information on the systems' thermal response. Knowing the thermal response of any HVAC system is important because it dictates the characteristics that its control strategy must have to maintain occupant thermal comfort while maximizing energy efficiency. Therefore, we used Ning et al.'s (2017) classification system to define high thermal mass radiant systems (HTMR) for our investigation. We consider their classification of medium and slow response systems as HTMR, which includes TABS and ESS. The location of the tubing is a key indicator in determining if it is a TABS or ESS and if it is considered a ceiling or floor system. TABS has the tubing embedded inside the structural floor/ceiling slab. In contrast, ESS has an insulating layer that thermally decouples the building structure from the radiant layer containing the tubing as shown in Figure 1. Both types of HTMR will transfer heat through the ceiling and floor surfaces. Albeit, ESS and TABS with insulation will observe a greatly reduced heat transfer on the backside surface (i.e. the surface further

https://doi.org/10.1016/j.enbuild.2025.115387
escholarship.org/uc/item/3812p9p1

away from the tubing) due to the insulation layer. Therefore, the radiant system is referred to as a ceiling or floor system, depending on the designed dominant heat transfer surface. For example, it is a ceiling radiant system if the ceiling surface is the dominant heat transfer surface by moving the tubing closer to the ceiling surface, as shown on the zone schematic on the right in Figure 1. Similarly, if the floor surface dominates heat transfer to the zone, it is considered a floor radiant system.

We focus on HTMR because of its slow thermal response to control actions. This attribute allows the decoupling of the cooling plant operation and the space cooling load profile to maintain thermal comfort. For instance, the cooling plant can operate during nighttime hours to precool the building's thermal mass. The space's heat gains are stored in the precooled thermal mass during occupied times to then be removed when the cycle repeats again. However, more research is needed to improve the definition of HTMR systems so strategies such as precooling can become standard. Ning et al.'s (2017) classification system only considers the radiant system without the thermal response of the whole space and its contents. The thermal response will also change depending on the characteristics of the space and internal heat gains. For example, the presence of a full or partial acoustical ceiling would have a large effect on overall zone response time even if the radiant system was identical.

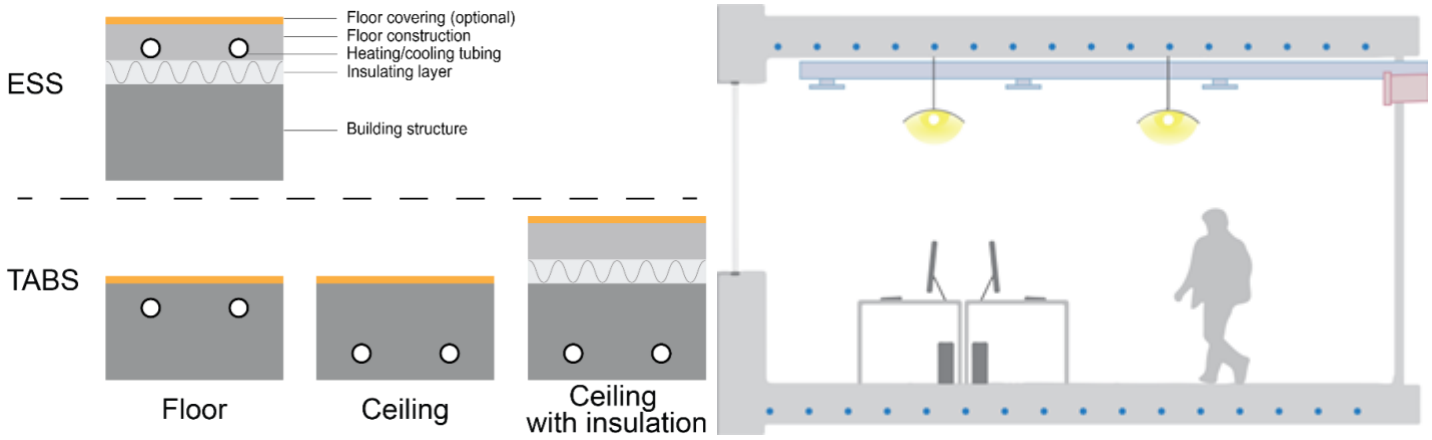

Figure 1: Left) Construction layers of high thermal mass radiant systems. Embedded surface systems (ESS) have an insulating layer that thermally decouples the structure from the radiant layer. Thermally activated systems (TABS) have the tubing embedded directly in the floor/ceiling building structural slabs. Right) Schematic of a typical zone with a TABS system with an overhead dedicated outdoor air system (DOAS) for ventilation. The tubing is depicted closer to the ceiling surface and would observe a higher heat transfer through the ceiling surface; thus, it is a TABS ceiling system.

The required SWT generally depends on the heat gains generated and entering the zone and the control strategy implemented in the radiant system, for example, the number of operation hours and water flow rate. A key advantage for radiant systems is the use of large heat transfer areas to compensate for the lower cooling capacity inherent in using higher than typical cooling water temperatures. Figure 2 shows a range of 4 to 26 °C for SWT used in previous laboratory, field, and simulation studies of RCP, ESS, and TABS. All studies constrained the peak operative temperature near 26 °C for the conditioned space. The bulk of reported SWTs are above 12 °C with a few low-temperature outliers. Figure 2 includes investigations where high-temperature cooling was used in mild and more extreme climates (Meierhans 1996; Stetiu 1999; Niu, Zhang, and Zuo 2002). In some climates, the SWT is often high enough that the space does not require any dehumidification. Still, an additional system is needed in hot and humid climates to address dehumidification and/or supplemental cooling (Zhang and Niu 2003). A DOAS system can be appropriately sized for dehumidification or oversized to provide supplemental cooling.

https://doi.org/10.1016/j.enbuild.2025.115387
escholarship.org/uc/item/3812p9p1

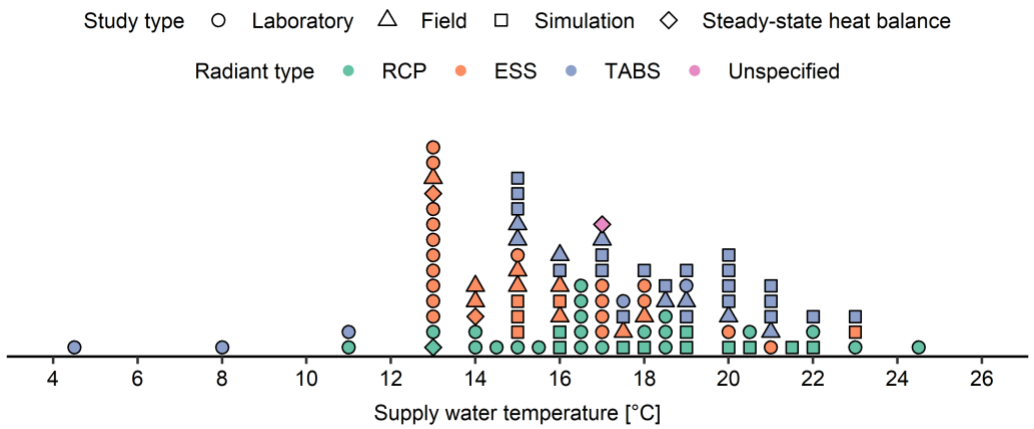

Figure 2: Supply water temperature (SWT) used in select laboratory, field, and simulation studies with radiant ceiling panels (RCP), embedded surface systems (ESS), and thermally activated building systems (TABS). Each symbol represents one experiment in which multiple experiments may be contained within one manuscript. We place the reported SWT in the graph to the nearest 0.5 °C.

Paliaga et al. (2017) showed that in North America, building designers rarely design cooling plants for HTMR that generate warmer temperatures or operate them in nighttime hours when more favorable weather or utility rate conditions exist. Knowing the warmest SWT allows building designers to evaluate if sustainable cooling plant options are adequate for a specific set of building characteristics and climate (Samuel, Nagendra, and Maiya 2013). One sustainable and probably cost-efficient option is to integrate adiabatic evaporative cooling with cooling towers or fluid coolers for cooled water production. A building can either exclusively rely on evaporative cooling for its cooling plant or use chillers designed with waterside economizing. Chillers with an integrated waterside economizer contain a heat exchanger piped in series with the chillers to precool the return water temperature (RWT). This waterside economizing method increases the number of economizing hours for the cooling plant and has less disruptive controls (Taylor 2014). Radiant systems that take advantage of waterside economizing have the potential for significant energy savings in the range of 8-15% (Niu, Kooi, and Rhee 1995), 10-20% (Sodec 1999), 21-23% (Raftery et al. 2012), and up to 55% (Tian and Love 2009) when compared to all-air systems. When using evaporative cooling exclusively, designers must consider the potential impacts on occupant thermal comfort since cooled water production with this process depends on weather conditions. Moreover, favorable weather conditions are usually not in sync with the required space cooling load profile. It is also reliant on the efficacy of the evaporative cooling equipment to approach the wet-bulb temperature (Wang, Niu, and van Paassen 2008). In short, high SWT enabled by HTMR shows potential to increase cooling efficiency but there is a lack of design guidelines for building designers to implement this design strategy in various US climates. Therefore, we systematically investigate the warmest SWT that maintains comfortable space temperatures when using HTMR with DOAS. Thus, in this paper, the objectives are:

1. To determine the warmest SWT that HTMR can use in various US climate zones and building designs during the cooling design day.
2. To determine if climate zones' outdoor dry and wet-bulb temperatures can produce the resulting SWT through adiabatic evaporative cooling using cooling towers or fluid coolers.
3. To calculate a climate zone's potential to operate waterside economizing through HTMR with DOAS systems.

2. Methods

We created single zone EnergyPlus models that use HTMR as the primary heating and cooling system. A dedicated outdoor air system (DOAS) supplies ventilation to the zone. We used a combination of full factorial design and quasi-random sampling (Sobol 1976) to define 360,900 models for simulation with different building and radiant system design parameters. Section 2.4 contains further details on the sampling method. EnergyPlus implements the full ASHRAE Heat Balance method (ASHRAE 2017) and has a validated radiant system module (Chantrasrisalai et al. 2003). The single zone represents a middle floor perimeter or core zone of an office building. For the perimeter zone, there is one window without shading on one façade, which represents the exterior wall. The opposite wall and the two side walls of the zone have an adiabatic boundary condition. For the core zone, all walls have an adiabatic boundary condition. In both zone types, the floor and ceiling are thermally interconnected to represent the heat transfer scenario of a middle floor within a larger building with multiple floors.

We used the Python eppy package to create all the energy models programmatically with the corresponding design parameters obtained from the Sobol' sampling method (Philip 2016). We used Python scripts to programmatically call the EnergyPlus simulation engine, collect results, and perform preliminary summary analysis. We used the R Statistical Software with the tidyverse package to conduct a more detailed analysis and generate plots (Wickham et al. 2019). We also used Python scripts to modify the SWT as needed in each iteration, as described in section 2.5. We performed the EnergyPlus simulations on the AWS platform using Ubuntu 18.04 LTS. We leased four c5d.18xlarge instances, with each instance having 72 virtual CPUs, 144 Gibibytes (GiB, 1 GiB is equal to 1.074 gigabytes), and 1,800 gigabytes (GB) of local storage. The simulations took about 2.5 days to complete, running in parallel using all the vCPUs. We used EnergyPlus version 9.3.

2.1. Envelope

The exterior wall of the zone is a metal-framed wall with four layers: in order from the outside to inside: stucco, insulation, metal frame with insulation batt, and gypsum board. Table 1 contains the layers' thermophysical properties. We adjusted the thickness and, by extension, its corresponding thermal resistance of the insulation layer in order for the whole wall assembly to meet the maximum U-factor allowed in the prescriptive requirements of the climate zone where the energy model is simulated; Title 24-2016 for California climate zones and ASHRAE 90.1-2016 for the rest of the US climate zones (ASHRAE 2016; CEC 2015). Similarly, the window's maximum U-factor and minimum solar heat gain coefficient (SHGC) are based on the climate zones' energy code. The maximum window-to-wall ratio (WWR) allowed in the prescriptive requirement is 40%, but we varied it from 20 to 60% for perimeter zones in this study. High WWR without shading is not typical for radiant systems due to their limited cooling capacity. However, we did not model shading in this study for simplicity, but its effects can be approximated by referencing lower WWR. Also, unprotected high WWR is not desirable due to the strong adverse effects of direct solar radiation on occupant thermal comfort and visual glare (Arens et al. 2015; Tuaycharoen and Tregenza 2016), as well as poor energy performance.

We used the quasi-random sampling method to test various zone lengths, widths, and orientations (Sobol 1976). Table 2 shows the lower and upper limits of the sampling method for each of the parameters. The zone length refers to the measurement that is parallel to the window length and zone width to the measurement going into the zone, i.e. perpendicular to the window. The zone height remains constant at 3 m for all test cases.

Table 1: Exterior wall construction layers with thermophysical properties.

Material	Thickness [m]	Thermal conductivity [$W \cdot m^{-1} \cdot K^{-1}$]	Specific heat [$J \cdot kg^{-1} \cdot K^{-1}$]	Density [$kg \cdot m^{-3}$]	Total R-value [$m^2 \cdot K \cdot W^{-1}$]
Stucco	0.0222	0.72	840	1856	0.0308
Insulation	a	0.032	1680	72	a
Metal frame with insulation batts	-	-	-	-	1.3
Gypsum board	0.0127	0.16	1090	800	0.79

a. Adjusted to meet energy code U-factor wall assembly requirement.

2.2. Internal heat gains

We sampled lighting (LPD) and plug load power densities (PLDP), and occupant density (OD) to define each model in this study. We used a constant radiant fraction for LPD that corresponds to LED lighting fixtures. The upper limit for LPD is the minimum allowed in office building types in ASHRAE 90.1-2016. Non-regulated internal heat gains include PLPD and OD. Title 24 Nonresidential ACM Reference Manual and US Department of Energy's (DOE) large office prototype building model informs limits on non-regulated loads (CEC 2016; Deru et al. 2011). The occupancy hours in the models are set to 8:00 to 18:00. We obtained the LPD, PLPD, and OD schedules from DOE's large office prototype building model. However, the factors' magnitude in these schedules are likely overestimated (Duarte, Van Den Wymelenberg, and Rieger 2013), which will result in conservative high-temperature cooling SWT values for typical days. However, it is appropriate for design day simulations. We modified the PLPD's after-hour schedule (18:01 to 7:59) to test different nighttime base loads of the zone. The sampled diversity factors are from 0.1 to 0.5 of the design PLPD.

The ventilation rates set in the models for all California climate zones are the maximum of 7.08 $L \cdot s^{-1}$ per person or 0.762 $L \cdot s^{-1} \cdot m^{-2}$ as defined in Title 24-2016. For all other US climate zones, the ventilation rates are the sum of 2.5 $L \cdot s^{-1}$ per person and 0.3 $L \cdot s^{-1} \cdot m^{-2}$ per ASHRAE 60.1-2016. We then used the sampling method to vary the ventilation rate up to two times the defined minimum value. A 30% above minimum ventilation airflow rate is common practice for DOAS and other ventilation systems to receive credits under rating systems such as LEED and WELL (Paliaga et al. 2017; USGBC 2020; IWBI 2021). Designing DOAS systems above minimum ventilation airflow rates may also provide supplementary cooling. The DOAS ventilation system in the models has dual temperature setpoints at 15 and 21 °C with a design outdoor humidity ratio sampled from 0.0128 and 0.0175 $kg_w \cdot kg_{da}^{-1}$. The design humidity ratio range corresponds to a dew point temperature range of 14.7 to 22.7 °C. It is important that the DOAS system's SWT be temperature independent or completely decoupled from the cooling plant serving the HTMR to increase the HTMR's SWT and its energy efficiency when applicable. A packaged air conditioning system or small chiller with or without a recovery system to only serve the DOAS would achieve the separation (Zhang 2006). Alternatively, a water-to-water heat pump could serve the DOAS system when colder temperature water is required for the radiant system, and a bypass allows for operation for the remainder of the year. Similarly, a desiccant dehumidification system may be used for ventilation air conditioning to maintain the goal of no vapor compression in the building design (Niu, Zhang, and Zuo 2002; La et al. 2010). In this study, the DOAS is a constant volume packaged air terminal unit for simplicity. We set the infiltration rate to 0.537 $L \cdot s^{-1} \cdot m^{-2}$ of exterior surface, which reduces to 0.134 $L \cdot s^{-1} \cdot m^{-2}$ when the ventilation system operates and pressurizes the building. The infiltration rate is in line with US commercial reference models (Deru et al. 2011).

2.3. Radiant system

We included a couple of radiant system design parameters in the full factorial design portion of defining the test cases while sampling other parameters using the quasi-random method described below. The radiant system design parameters included in the full factorial are radiant system type (ESS-floor, TABS-floor, TABS-ceiling, TABS-insulation) and tube spacing (0.1524, 0.2286, 0.3048 m). Since the ESS-ceiling radiant system type is not a common design choice, we decided to instead include a TABS-ceiling containing an insulation layer (TABS-insulation) as shown on the left hand side in Figure 1. This is a more common design choice as the insulation layer helps thermally decouple spaces and/or reduce footfall noise. We treated the tube spacing as a discrete parameter because PEX tubing manufacturers have standardized tube mats and other products to these three spacing lengths. We simulate the four levels in the radiant system type and main active surface, as shown on the left hand side in Figure 1, and tube spacing because these factors are standardized options in the HTMR design and have significant effects on its performance. The rest of the parameters studied here have considerable variation among building projects, and this is why we chose to sample within a range.

We sampled: floor/ceiling slab thickness; tube depth; outside tube diameter; maximum circuit, or 'loop' length; slab and floor construction thermal conductivity; floor covering thermal resistance; design supply/return temperature difference; radiant system operation start time; and radiant system operation duration. Since the sampling method treats slab thickness and depth as independent parameters, it is possible to pair them up in nonrealistic ways, e.g. a tube depth of 0.1524 m with a slab thickness of 0.1016 m. Thus, we deleted test cases where tube depth exceeded slab thickness or was not within typical manufacturer-recommended bounds (e.g., embedded piping should be at least 2.54 cm from a ceiling or floor surface). The tube depth is the measurement from the main active surface (i.e., the surface with the dominant heat transfer) to the top of the tube. Tube diameters also come in discrete sizes, but we wanted to test a range of diameters without adding extensive test cases to this simulation study. Instead, we reference tube diameter specifications in ASTM standard F876-2017 and used linear interpolation to define non-standard tube diameters (ASTM 2017). We assumed the same thermal conductivity for the building slab structure and floor construction, e.g. topping layer, with constant specific heat and density of 900 $J \cdot kg^{-1} \cdot K^{-1}$ and 2,240 $kg \cdot m^{-3}$, respectively.

We calculated the total volumetric water flow rate through the radiant system by performing a steady-state heat balance between the hydronic heat transfer and the radiant system design capacity according to ISO standard 11855-2012, as shown in Equation 1 (ISO 2012), where $\dot{V}_{tlt}$ is the total volumetric flow rate, q_{ISO} is the design capacity according to ISO standard 11855-2012, ρ and c_p are the density and specific heat of the fluid flowing through the radiant system, respectively. One of the inputs to the ISO design capacity calculation is SWT. Since this is an unknown parameter in this study, we defined a reference SWT at 12.8 °C to determine the steady-state design capacity used to calculate $\dot{V}_{tlt}$. However, we maintained the same calculated $\dot{V}_{tlt}$ for each test case throughout the iteration process of finding the final SWT. For ESS, we used ISO method for Type A and C in Appendix A of ISO standard 11855-2012 and Type E in Appendix B of the standard for TABS. We also created a web tool (CBE Rad tool) to calculate these values, which is freely available (Raftery et al. 2019).

$$\dot{V}_{tlt} = \frac{q_{ISO}}{\rho c_p (RWT - SWT)} \qquad \text{Equation 1}$$

https://doi.org/10.1016/j.enbuild.2025.115387
escholarship.org/uc/item/3812p9p1

We determined the total tube length in each test case using the zone tube spacing and the total area, using the assumption of an average 10% leader length for connecting back to the radiant manifold. Then, we calculated the number of loops in each test case by dividing the total tube length by the maximum loop length and rounding up to the next whole loop. Thus, the actual loop length used for simulation is lower than the sampled maximum loop length. Next, we calculated the pressure drop per loop at the steady-state design condition using the Darcy-Weisbach equation and the Swamee-Jain friction factor. We iteratively increased the number of loops if the pressure drop per loop exceeded manufacturer recommendations (30 kPa). We used water as the fluid through the radiant system.

We sampled radiant system operation start time and number of operating hours in a 24-hour period to create various combinations of these two factors that would represent many different design day control strategy scenarios. Every building is unique and may require different operation times of their HVAC system due to utility price tariff structure, availability and time-dependent efficiency of the central cooling plant, or other constraints. We sampled the start time from integers 0-23 representing an hour of the day from midnight to 23:00 while the operation duration from integers 8-24. Thus, there are 408 possible design day control strategy scenarios that the HTMR can operate. In practice, a building designer may opt to implement typical control strategies which include nighttime precooling, afternoon shutoff, or 24-hour operation (Raftery et al. 2017). Finally, we defined the cooling plant as a district cooling object in EnergyPlus to supply the requested water temperature to the HTMR during all its operation period, i.e. unlimited cooling plant capacity. This hydronic system is classified as a constant temperature, constant flow rate system and operates in this manner during the cooling design day.

2.4. Sampling method

We used Sobol' quasi-random sequences to sample all parameters listed in Table 2 (Sobol 1976). This sampling method is not performing a truly random sample of parameters since it has knowledge of the previously sampled points to avoid clusters and gaps (Saltelli et al. 2010). The method progressively samples the space at a given density, thus requiring a sample size of 2^m points (m=1,2,…) where a higher chosen *m* increases the density of sample points in the space. Sobol' sequences outperformed other Monte Carlo sampling methods when evaluating a simple building simulation model, and all tested sampling techniques converged with a sample size of 256 points, i.e. an *m* equal to eight (Burhenne, Jacob, and Henze 2011). However, upon closer inspection of the resulting sampling with a sample size of 256 on 19 parameters, we found poor two-dimensional projections between some parameters. We used the algorithm outlined in Joe and Kuo (2008) to mitigate this issue and increased *m* up to 10.

As mentioned earlier, we performed a full factorial design on some parameters, listed in Table 3. Furthermore, we implemented different sample sizes for perimeter (1024) and core (64) zones to reduce the total number of cases to simulate. We sampled fewer core zones because these zones are unlikely the driving force behind a warmer SWT design for the HVAC system and have less heat gain variation due to the absence of direct solar heat gains and wall loads. The full factorial design results in 360 test cases for each perimeter and core zone type. Factoring in the sample size for using Sobol' sequences on each zone type results in 368,640 test cases for perimeter and 23,040 for core zones. We deleted 30,780 test cases where the tube depth exceeds slab thickness or is not within specified bounds. In total, we created 360,900 single zone models that went through the cooling design day simulation. After the simulations, we identified test cases where condensation issues occurred in the space. We recorded these test cases as NA. Condensation issues occur when the SWT is at or below the space's dew point temperature. We only remove test cases with

condensation issues from the main analysis but use the remaining data in our various analyses to make proper assessments of the limitations of the different building and HTMR design parameters we tested. Supplementary material 'a' contains further details on the test cases that would not be implemented in practice due to condensation issues, thermal comfort bound not met, and below typical all-air SWT. We also refer to the typical all-air SWT as "HVAC industry ChW".

Table 2: Lower and upper limits in which continuous design parameters for each of the models could be sampled.

Design parameter	Lower limit	Upper limit	Additional notes
Window-to-wall ratio	20	60%	Only for perimeter zone
Zone length	3	45 m	Measurement parallel to window length
Zone width	3	9 m	Measurement into zone
Exterior wall orientation	0	359°	South = 0° | West = 90° North = 180° | East = 270°
Lights	5	8.5 $W \cdot m^{-2}$	Radiant fraction = 0.72
Plug loads	5	14 $W \cdot m^{-2}$	Radiant fraction = 0.5
Floor area per occupant	5	20 $m^2 \cdot person^{-1}$	Radiant fraction = 0.4
Nighttime plug load diversity factor	0.1	0.5	-
Ventilation oversize airflow factor	1	2	-
Supply air design humidity ratio	0.0128	0.0175 $kg \cdot kg^{-1} \cdot$dry air	-
Floor/ceiling slab thickness	0.1016	0.3048 m	-
Tube depth	0.0254	0.1524 m	Measurement is taken from the main active surface to the top of the tube
Outside tube diameter	0.0127	0.02858 m	Includes non-standard diameters
Maximum loop length	45.7	152.4 m	-
Slab and floor construction thermal conductivity	1	2.5 $W \cdot m^{-1} \cdot K^{-1}$	-
Floor covering thermal resistance	0	0.35 $m \cdot K \cdot W^{-1}$	-
Supply/return temperature difference	1.67	8.3 °C	-
Radiant operation start time	0:00	23:00	-
Radiant operation duration	8	24 h	-

Table 3: Summary of design parameters for full factorial design.

Design parameter	Levels
Climate zone	1 to 30 (14 US climates and 16 California)[a]
Zone type	Perimeter, Core
HTMR type	ESS-floor, TABS-floor, TABS-ceiling, TABS-insulation
Tube spacing	0.1524, 0.2286, 0.3048 m

a: Climate zones used for simulation: ASHRAE Standard 196-2006: 1A-Miami, FL, 1B-Phoenix, AZ, 2A-Houston, TX, 2B-Las Vegas, NV, 3A-Atlanta, GA, 4A-Baltimore, MD, 4A-Seattle, WA, 4B-Albuquerque, NM, 4B-Boise, ID, 5A-Chicago, IL, 6A-Minneapolis, MN, 6B-Helena, MT, 7-Duluth, MN, 8-Fairbanks, AK;
California: 01-Arcata (ASHRAE climate zone: 4A), 02-Santa Rosa (3C), 03-Oakland (3C), 04-San Jose (3C), 05-Santa Maria (3C), 06-Torrance (3C), 07-San Diego (3A), 08-Fullerton (3A), 09-Burbank (3A), 10-Riverside (3B), 11-Red Bluff (3C), 12-Sacramento (3C), 13-Fresno (3A), 14-Palmdale (3B), 15-Palm Springs (2B), 16-Blue Canyon (5C)

2.5. Supply water temperature calculation and analysis

We calculated thermal comfort bounds using an operative temperature range of 22.5 to 26 °C. This corresponds to ±0.5 predicted mean vote (PMV) at an airspeed of 0.1 m·s^{-1}, relative humidity of 50%, occupant metabolic rate of 1.2 MET, and clothing insulation of 0.57 clo. We used the upper thermal comfort limit of 26 °C with a tolerance of ±0.25 °C as the stopping criteria for searching the required SWT to the HTMR.

We initialized the SWT for each model using predictions from Duarte et al.'s (2018) random forest model on SWT for TABS. The nonlinear model requires instantaneous peak heat gain rate, WWR, exterior wall orientation, slab thickness, tube depth and spacing, and HTMR start time and operation hours in a 24-hour period. We calculated heat gain rates for solar, internal, envelope, ventilation, and infiltration according to ASHRAE's 2017 Handbook of Fundamentals (ASHRAE 2017) to obtain heat gain rate estimates to feed into Duarte et al.'s (2018) random forest models. We outlined our assumptions for heat gain rate calculations in Supplementary material 'b'.

Once we obtained the initial SWT, we simulated the models and extracted the maximum operative temperature in each zone during occupied hours. If the operative temperature for a specific test case was not within ± 0.25 °C from the upper thermal comfort limit, we adjusted its SWT per Equation 2 and repeated the simulation. This step was iterated until the maximum operative temperature for each model was within ± 0.25 °C or SWT adjusted below the default plant loop minimum temperature in EnergyPlus which is 3 °C. It may be possible that zone operative temperature is not within thermal comfort bounds for test cases that stopped when the plant loop minimum was reached.

$$\begin{aligned} SWT_n &= SWT_{n-1} + 1.0\varepsilon \quad if\ \varepsilon > 3\eta \\ SWT_n &= SWT_{n-1} + 0.8\varepsilon \quad if\ 2\eta < \varepsilon \leq 3\eta \\ SWT_n &= SWT_{n-1} + 0.6\varepsilon \quad if\ \varepsilon \leq 2\eta \end{aligned} \qquad \text{Equation 2}$$

The subscripts n and $n-1$ in Equation 2 represent the new and old SWT, respectively, ε represents the error, and η the tolerance set at 0.25 °C. The error (ε) is calculated as the difference between the upper comfort bound and the maximum operative temperature during occupied hours calculated in the simulation. This is conceptually similar to a control strategy presented in Raftery et al. (2017). The only parameter changing between each simulation iteration is the SWT to the radiant system; everything else remains constant, including the water flow rate through the radiant system tubes.

We analyzed the simulation results to extract trends and information to develop HTMR design guidance for building designers. Although developing a simplified prediction model is not part of the scope of this study, we used machine learning techniques on the resulting simulation data to extract the most important input parameters that impact the prediction of SWT and the mean hydronic heat extraction (HX) rate during cooling plant operation. We first used recursive feature selection with random forest regression models to generally remove redundant and weak predictors for SWT and hydronic HX rate (Chen and Jeong 2007). Then, we used the stochastic gradient boosting algorithm to identify input parameters that have interaction effects between them that improve prediction results (Friedman 2002). We evaluated interaction effects in groups of three parameters. We used most of the input parameters listed in Table 2 and Table 3 in these machine learning analyses. We simplified sensible heat gain rates expected to be removed by the radiant obtained from the simulation results into peak and 24-hour mean values and combined zone width and length into an aspect ratio for input into the machine learning techniques to find important prediction input parameters. We also

did not include climate zone but added the parameters site latitude, water flow rate per loop, water flow rate per floor area, water flow rate-loop per floor area, and water flow velocity. We ran these machine learning analyses using the R Statistical Software with the package caret using about 51,000 EnergyPlus simulation test cases to minimize computational time (Kuhn 2008). Furthermore, we performed the training with three repeated, ten-fold cross-validation.

2.6. Outdoor wet bulb temperature analysis

We downloaded design day information and annual weather files from EnergyPlus's website to do the analysis for this study including the comparison between the required SWT in the test cases and wet-bulb temperature (DOE 2018). However, wet-bulb temperature is not included in the weather files, so we calculated it using the Python module CoolProp (Bell et al. 2014). We arbitrarily selected May through the end of October to create a subset of annual wet-bulb temperature to include the majority of the cooling season. It is essential to compare wet-bulb temperature to SWT because wet-bulb temperature is an important driver for cooling towers and fluid coolers to generate the needed cooled water. The lower the wet-bulb temperature, the lower the temperature of the cooled water and the higher the percentage of building and radiant design variants that can provide comfortable temperatures by only using adiabatic evaporative cooling. The outgoing water temperature from conventional cooling towers and fluid coolers will not equal the climates' wet-bulb temperature. The primary approach temperature – the difference between the wet-bulb temperature and the outgoing cooling tower water temperature – can be 1-2 °C and an additional 2-4 °C for the secondary approach temperature – the difference between the outgoing cooling tower water temperature and the SWT into the radiant system – due to a heat exchanger for the cooling tower in low-temperature rejection applications (Costelloe and Finn 2003). However, advances in fluid coolers have made it possible to produce outgoing water temperatures lower than the climate zone's wet-bulb temperature and approach the dewpoint temperature (Mahmood et al. 2016; Sverdlin, Tikhonov, and Gelfand 2011). For simplicity, when we refer to approach temperature for the rest of this paper, it is meant to signify the sum of the primary and any secondary approach temperatures.

We compare the wet-bulb temperature and SWT distributions using box and whisker plots for each climate zone. The box portion of the plot represents the interquartile range (IQR) (25^{th}-75^{th} percentiles) with the median presented with a solid black horizontal line inside the IQR. The tips of the upper and bottom whiskers represent the 90^{th} and 10^{th} percentile, respectively. We use the same definition whenever we use box and whisker plots to visualize data results. On some occasions, we dropped the whiskers to increase the readability of the plot.

We can qualitatively assess the wet-bulb temperature and SWT distributions by observing the difference between the two distributions. The further the SWT distribution is above the wet-bulb temperature distribution, the more hours of the cooling season that evaporative cooling equipment can meet the primary space cooling requirements. In some climates, it is feasible to design a building's cooling plant only using evaporative cooling for the primary cooling requirements of the building's spaces. To assess this quantitatively, we calculated the number of potential waterside economizing hours for each test case. For each test case, we subset the climate zone's wet-bulb temperature during the cooling season to coincide with only the cooling plant's hours of operation, added a constant approach temperature to the wet-bulb temperature, and counted the total number of hours where the SWT was greater than the wet-bulb temperature plus the approach temperature. We used approach temperatures of 0, 2, 4, and 6 °C to consider various performance levels of evaporative cooling devices. Since the number of cooling plant operation hours

on the design day varies among the test cases, we divided the resulting economizing hours by the number of hours the cooling plant would potentially operate during the cooling season to represent economizing hours as a percentage of total cooling plant operation. Furthermore, we calculated and reported the median percentage of economizing operation for each approach temperature and climate zone.

3. Results

The aggregate summary statistics include maximum, 24-hour mean, and occupancy-hours-only mean on various parameters useful for the design of HTMR. However, it is important to keep in mind that individual test cases contain timeseries results that change throughout the course of the design day and HTMR systems do not reach a steady-state condition due to their inherent thermal inertia. Appendix A contains visualizations and a discussion of the timeseries results of two example cases highlighting this issue in more depth.

3.1. Test cases with low supply water temperature

We created 360,900 total energy models. We removed 4,952 models due to EnergyPlus flagging them with condensation issues. There are 355,948 models remaining on which we perform our analysis on. Of the remaining simulation results, 56,114 resulted in unrealistic cases primarily due to unrealistically low SWT (below 7.2 °C) including test cases that reached the minimum plant loop temperature. A significant number of simulations (93,695) resulted below typical SWT for HTMR (12.8 °C). We extracted the simulated heat gain rate of the zones to compare the total 24-hour cumulative simulated heat gain energy to the total 24-hour cumulative design hydronic HX energy (Q_{hyd}) as calculated in Equation 3.

$$Q_{hyd} = 3600\left(\dot{V}_{tlt}\rho c_p \Delta T_{r-s} \Delta t_{hyd}\right) \quad \text{Equation 3}$$

Where $\dot{V}_{tlt}$ is the total volumetric water flow rate as calculated in Equation 1, ΔT_{r-s} is the design supply/return temperature difference, and Δt_{hyd} is the HTMR operation duration hours. Q_{hyd} is calculated before any simulation is performed so it is not the hydronic HX energy resulting from the design day simulation in EnergyPlus. Using non-simulated and high-level data will allow practitioners to assess high-temperature potential in early design where only back of the envelope calculations are available.

Figure 3 shows the distribution of a metric we call ΔR_{X-G} and calculated using Equation 4. ΔR_{X-G} is the difference between Q_{hyd} and simulated sensible heat gain ($HG^{sen}_{sim_{zn}}$) energy introduced in the zone as a percentage of Q_{hyd} and it is used to gain information on why models requested low SWT for their radiant system. $HG^{sen}_{sim_{zn}}$ energy is the 24-hour sum of sensible heat gain energy into the zone due to people, lights, plug loads, net window gain or loss, net wall gain or loss, and net gain or loss due to the introduction of conditioned ventilation air into the zone at the corresponding dry-bulb air temperature for each timestep. The assumption is that the resulting heat gain energy of this addition is to be extracted by the radiant system.

Figure 3 suggests that $HG^{sen}_{sim_{zn}}$ were too high for the cooling plant where SWT resulted below 7.2 °C in the model given the water flow rate and the operation schedule. Designers can calculate ΔR_{X-G} using estimated zone sensible heat gain and cooling plant HX energy in a 24-hour period for their building and HTMR designs and use Figure 3 to get a preliminary estimate of the range of SWT needed. Warmer SWT are possible as ΔR_{X-G} becomes positive. A negative number suggests that the radiant hydronic system may be undersized, its operation duration is insufficient, heat gain rates in the space are too high, or a combination of these issues.

$$\Delta R_{X-G} = \left(\frac{Q_{hyd} - HG^{sen}_{sim_{zn}}}{Q_{hyd}} \right) \quad \text{Equation 4}$$

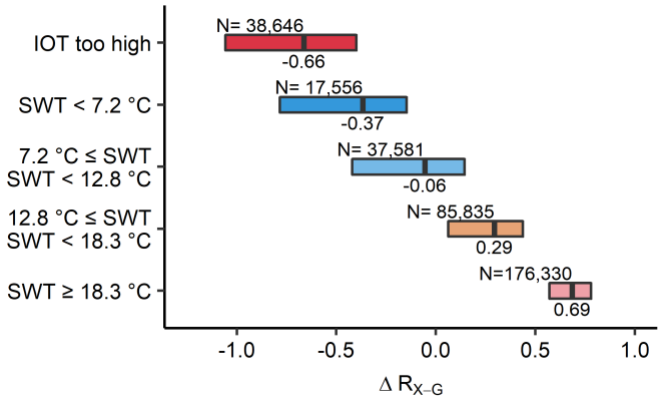

Figure 3: Comparison between 24-hour design hydronic heat extraction energy and simulated heat gain energy on the cooling design day by using the ratio ΔR_{X-G} calculated with Equation 4. A negative number suggests that the radiant hydronic system might be undersized, its operation duration is insufficient, heat gains in the space are too high, or a combination of these issues. N indicates the number of total test cases in each distribution. The first distribution in red represents test cases where peak design indoor operative temperature (IOT) was not met. Distributions do not include test cases with reported condensation problems.

Moreover, 88% of the test cases that resulted in SWT below 12.8 °C effectively only have one active surface to remove heat gains, i.e., ESS-floor and TABS-insulation. Additional filtering shows that ESS-floor has a greater proportion of test cases (57%) with SWT below 12.8 °C since a floor surface's convective heat transfer coefficient is smaller than a ceiling surface in cooling mode (Rhee and Kim 2015). Table 4 shows the peak and 24-hour mean $HG^{sen}_{sim_{zn}}$ rates that each HTMR type can extract with a 12.8 °C SWT and still maintain comfortable zone temperatures. HTMR designers should use Table 4 as upper limits for zone sensible heat gains rates allowed for high-temperature cooling with HTMR. Table 4 and Figure 4 show the significant limitation of ESS-floor to extract high levels of heat gains with warmer than typical SWT. In addition, they show that TABS-floor and TABS-ceiling perform similarly. For this reason, we will combine TABS-floor and TABS-ceiling data into one TABS category for subsequent analysis to have three HTMR categories.

Table 4: Maximum zone sensible heat gain ($HG^{sen}_{sim_{zn}}$) rates allowed for high-temperature cooling with high thermal mass radiant (HTMR). Median and first and third quartile $HG^{sen}_{sim_{zn}}$ rates at which each HTMR can extract with a 12.8 °C supply water temperature.

HTMR type	Peak $HG^{sen}_{sim_{zn}}$ Q2 (Q1, Q3) [W·m^{-2}]	24-hour mean $HG^{sen}_{sim_{zn}}$ Q2 (Q1, Q3) [W·m^{-2}]
ESS-floor	31 (24, 39)	12 (10, 14)
TABS-floor	76 (62, 94)	27 (22, 31)
TABS-ceiling	78 (63, 96)	27 (22, 32)
TABS-insulation	50 (38, 64)	18 (15, 22)

https://doi.org/10.1016/j.enbuild.2025.115387
escholarship.org/uc/item/3812p9p1

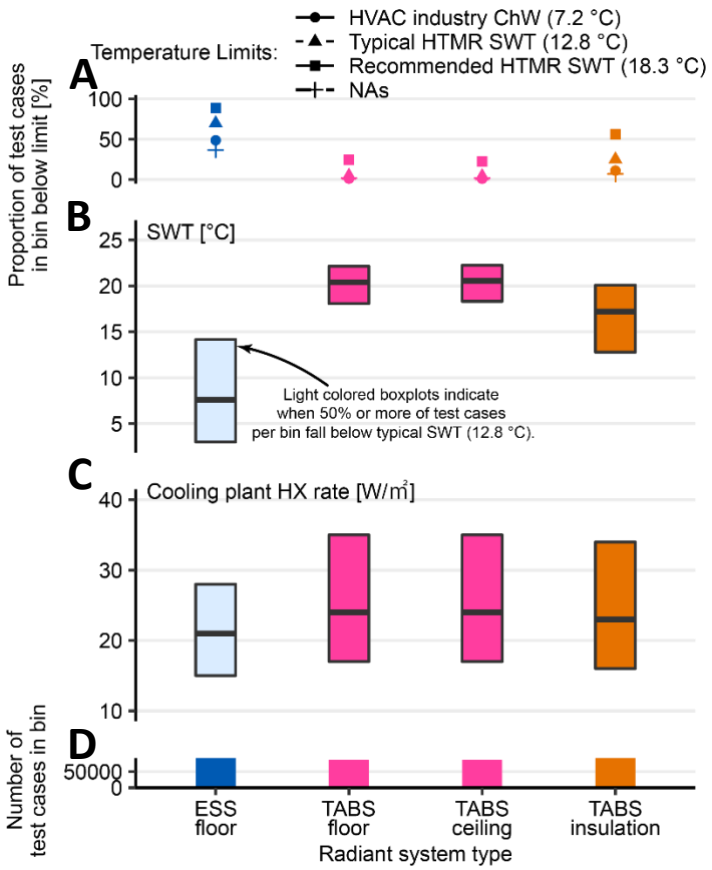

Figure 4: A) Proportion of test cases in each bin that are below various temperature limits: HVAC industry ChW and typical and recommended minimum supply water temperatures (SWT) for high thermal mass radiant systems (HTMR), B) SWT, C) cooling plant mean heat extraction (HX) rate during its operation duration, and D) number of test cases as a function of HTMR system type. Light colored boxplots indicate when 50% or more of the test cases per bin fall below typical HTMR SWT (12.8 °C).

3.2. High-level summary results

We report the following high-level results using the format: median (first quartile, third quartile). At an aggregate level, the resulting SWT for the test cases are 18.2 °C (12.3, 21.1) as Figure 5 shows. The resulting instantaneous simulated peak sensible heat gain rates entering or generated in the zones expected to be removed by the radiant system are 38 $W \cdot m^{-2}$ (26, 54). The test cases' peak surface HX rates are 30 $W \cdot m^{-2}$ (21, 42) and 23 $W \cdot m^{-2}$ (16, 32) for the mean hydronic HX rate during operation, i.e., cooling plant HX rate. On average, test cases with two active surfaces, i.e. TABS, can use SWT at least 4 °C warmer and can increase the peak active surface HX rate by at least 2 $W \cdot m^{-2}$ compared to test cases with one active surface, i.e. ESS-floor and TABS-insulation. ESS-floor has the largest difference between the two metrics when compared to TABS. Even though HTMR systems with only one active surface remove less heat gains from the space, there are still benefits from the second 'passive' surface if exposed. The exposed passive surface is radiatively cooled by the active surface and thus contributes substantially to the overall heat transfer and heat storage dynamics in the zone. The dynamics of an identical zone but with an unexposed passive surface, e.g. blocked with a drop ceiling, would perform very differently, especially in load shifting cases where the cooling happens at night. Table 5 shows additional summary statistics on select heat gain and HX rates broken down by radiant system type.

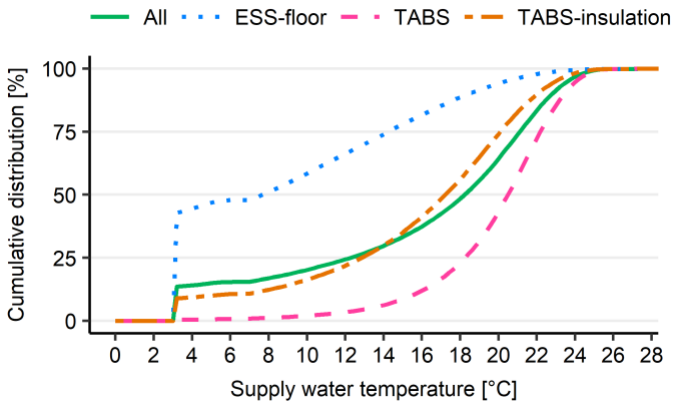

Figure 5: Cumulative distribution plot of the supply water temperature (SWT) for (All) 355,948 test cases without condensation issues, floor embedded surface systems (ESS-floor), thermally activated building systems with two active surfaces (TABS), and TABS with an insulation layer (TABS-insulation).

Table 5: Summary statistics, i.e. minimum (Min), first, second, and third quartile (Q1-Q3), average (Avg), and maximum (Max), for supply water temperature (SWT), heat gain (HG) rates, and heat extraction (HX) rates for remaining test cases after removing test case with condensation issues split by radiant type. ESS is further broken down by active surface.

	ESS-floor						**TABS**						**TABS-insulation**					
	Min	Q1	Q2	Avg	Q3	Max	Min	Q1	Q2	Avg	Q3	Max	Min	Q1	Q2	Avg	Q3	Max
SWT [°C]	3	3	7.7	8.9	14.2	28.3	3	18.3	20.5	19.8	22.2	28.4	3	12.9	17.2	15.8	20	28.4
Peak total HG [W·m^{-2}]	12	47	60	63	75	185	12	49	62	65	78	209	12	48	61	65	77	195
24 h mean total HG [W·m^{-2}]	4	19	23	24	28	60	4	20	25	26	30	71	4	20	24	25	30	67
Peak sensible HG expected to be extracted by radiant system [W·m^{-2}]	4	25	36	39	51	169	4	26	39	43	55	198	4	26	38	42	54	179
24 h mean sensible HG expected to be extracted by radiant system [W·m^{-2}]	-5	10	13	14	17	42	-5	11	15	16	20	64	-5	10	14	15	19	55
Peak active surface HX [W·m^{-2}]	2	20	29	31	40	121	2	22	31	35	44	156	3	21	30	33	42	135
24 h mean active surface HX [W·m^{-2}]	<1	10	13	14	17	43	<1	11	15	16	20	63	<1	11	15	16	20	58
Occupied h mean active surface HX [W·m^{-2}]	1	15	20	21	26	73	2	16	23	24	30	108	2	16	22	23	29	91
Peak total DOAS HX [W·m^{-2}]	4	14	21	23	31	90	3	13	20	23	30	88	4	13	21	23	30	88
Peak sensible DOAS HX [W·m^{-2}]	3	11	17	20	27	88	3	10	16	19	27	84	3	10	16	19	27	85
Peak HTMR cooling plant HX [W·m^{-2}]	0	18	26	27	35	92	0	20	31	35	45	198	0	18	26	30	39	149
24 h mean HTMR cooling plant HX [W·m^{-2}]	0	10	13	13	17	43	0	11	15	16	20	64	0	11	15	16	20	58
Operation h mean HTMR cooling plant HX [W·m^{-2}]	0	15	21	22	28	68	0	16	24	27	34	140	0	16	23	26	34	115

A negative number represents a net heat loss rate from the zone to the environment instead of a heat gain rate.

https://doi.org/10.1016/j.enbuild.2025.115387
escholarship.org/uc/item/3812p9p1

3.3. Waterside economizing operation potential

Figure 6 shows A) the median percentage of operating hours when waterside economizing is feasible for different approach temperatures, and B) the distribution of the resulting SWT for each climate zone. The results show that 21 climate zones out of 30 support at least 40% waterside economizing operation when using evaporative cooling systems with a 4 °C approach temperature. Four additional climate zones exceed the 40% waterside economizing operation threshold if higher performance evaporative cooling devices can be used such that the approach temperature is reduced to 2 °C. It is no surprise that Houston and Miami have the lowest waterside economizing potential given the high humidity. Even a high-performing evaporative cooling device with a 0 °C approach temperature will not increase waterside economizing operation for Miami. However, all climates, including hot and humid climates, benefit from using HTMR. The median of test cases with TABS-insulation uses 10 °C warmer SWT than the typical water temperature used for conventional chilled water systems serving all-air systems (typically 7.2 °C in the US). For TABS, the same metric increases to 13.3 °C. There is not a significant increase in SWT with ESS-floor systems which only gains a 0.5 °C.

https://doi.org/10.1016/j.enbuild.2025.115387
escholarship.org/uc/item/3812p9p1

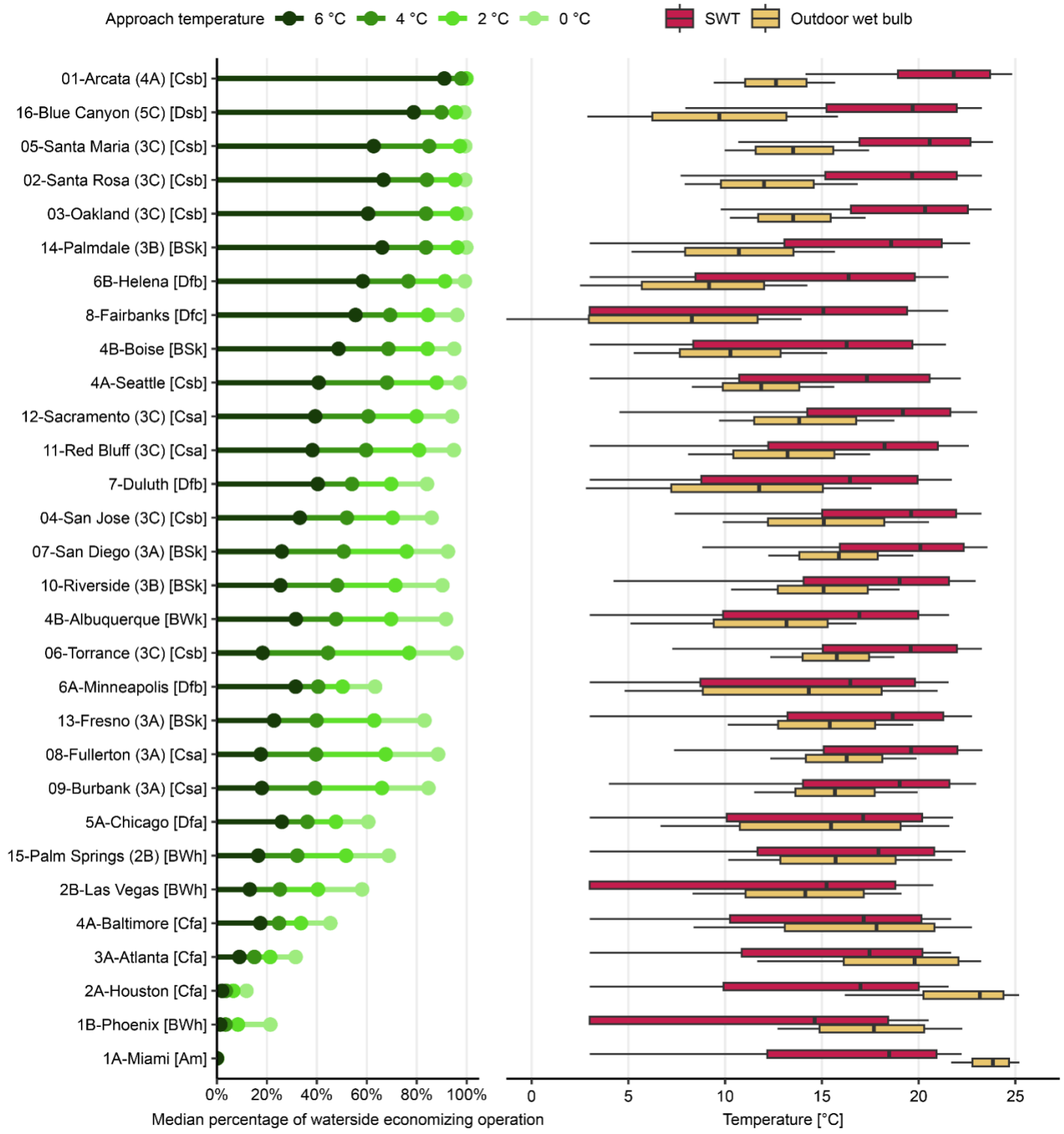

Figure 6: Left) The median percentage of operating hours during which waterside economizing is feasible for all test cases in each climate zone using various approach temperatures, and right) comparison of supply water temperatures (SWT) (red) distribution results with climate zone wet bulb temperature distribution (yellow) during the cooling season. The climate zones are sorted by decreasing waterside economizing operation for the 4 °C approach temperature. We refer to California's climate zones as California

https://doi.org/10.1016/j.enbuild.2025.115387
escholarship.org/uc/item/3812p9p1

climate zone number-representative city (ASHRAE climate zone). For US climate zones, we refer to them by ASHRAE climate zone-representative city. The Köppen-Geiger climate classification is in brackets for California and ASHRAE climate zones.

3.4. Parameter importance for supply water temperature and hydronic heat extraction

Figure 7 shows that the recursive feature selection analysis resulted in 18 parameters giving the best prediction performance for both SWT and hydronic HX rate normalized by floor area. The resulting root mean squared error (RMSE) of the best models are 0.88 °C and 0.85 $W \cdot m^{-2}$ for SWT and hydronic HX rate, respectively. However, reducing to 6 parameters to predict SWT or HX rate does not significantly decrease when compared to the best models' performance. Further improvements, in theory, can be made by adding additional data to the training process. Figure 7 also contains lists of the most important parameters ranked from greater to lesser importance (the first column contains the greater importance parameters). Active surface, radiant system operation duration, and temperature difference between simulated supply and return water temperature resulted in the most important parameters for SWT prediction. Operation duration and 24-hour mean sensible heat gain rate expected to be removed by the HTMR resulted in the most important for the hydronic HX rate prediction. The interaction effects analysis shows that the top 20 performing models include the following two important parameters for SWT prediction: water flow rate per area (found in 18 models) and 24-hour mean sensible heat gain rate (18). The mean RMSE among these 20 models is 3.2 °C. In the case of the hydronic HX rate, important parameters include operation duration (20) and 24-hour mean sensible heat gain rate (20). The mean RMSE for the top 20 hydronic HX rate models is 1.8 $W \cdot m^{-2}$.

As expected and shown in Figure 8, the more heat gains, the lower the SWT to the HTMR (and the higher the hydronic HX rate) needed to maintain thermally comfortable temperatures for the occupant. However, HTMR have limited HX capacity (Lehmann, Dorer, and Koschenz 2007). In this study, we observe that the median of test cases with TABS-insulation cannot extract 24-hour mean sensible heat gains of more than 18 $W \cdot m^{-2}$ or peak sensible heat gains of more than 50 $W \cdot m^{-2}$ with typical HTMR SWT of 12.8 °C. It is even less for ESS-floor systems with 12 and 31 $W \cdot m^{-2}$ for 24-hour mean and peak sensible heat gains, respectively. In the case of TABS, the limits increase to 27 $W \cdot m^{-2}$ and 77 $W \cdot m^{-2}$ for the 24-hour mean and peak sensible heat gains, respectively. The identification of important parameters suggests that the 24-hour mean sensible heat gain rate is more important than the peak sensible heat gain rate for the design of HTMR. The visualizations of the interaction between SWT, WWR, and orientation in Figure 9 show that core and north perimeter zones consistently required high SWT, even with increasing WWR in north perimeter zones with the exception of ESS-floor. For all other orientations, the required SWT decreases as WWR increases and at a faster rate for ESS-floor. The SWT in west-facing perimeter zones decreases the most as WWR increases, which is expected due to the difficulty of controlling solar heat gains towards the end of the day in this orientation when heat gains, in general, have been accumulating throughout the day. Somewhat counterintuitively, we can observe trends when plotting SWT against WWR or orientation, but it did not appear in the most important parameters for predictions. However, it may be due to most of the information is already captured through the 24-hour mean sensible heat gain parameter.

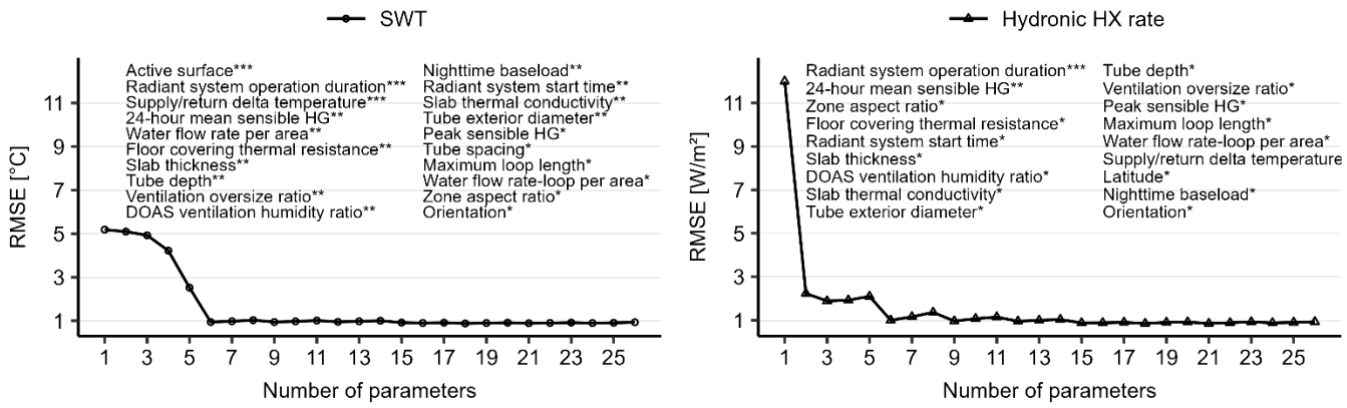

Figure 7: Results of the recursive feature selection analysis which shows the model prediction performance as more parameters are used for model training. The lists show 15 and 18 parameters for left) supply water temperature (SWT) and right) hydronic heat extraction (HX) rate normalized by floor area, respectively, that had the least error in the training predictions. The number of '*' represents the importance of the parameter with '***' being the highest.

Previous research has shown that the needed HTMR cooling plant capacity decreases as the number of hours the HTMR operates increases (Olesen and Zöllner 2007; Duarte et al. 2018). We also observe the same results (see Figure 10). Increasing the operation hours from 10 to 18 hours decreases the required cooling plant capacity by an average of 34%, 48%, and 46% for ESS-floor, TABS, and TABS-insulation, respectively and increases the required SWT by an average of 4 °C, 3 °C and 5 °C in ESS-floor, TABS and TABS-insulation, respectively. The reductions in cooling plant capacity can be an average of up to 61% and SWT increase up to 6 °C if the plant operates for the full 24 hours, but there is little flexibility in consistently avoiding unfavorable operation conditions such as high outdoor temperatures, high electricity prices, or high grid marginal carbon emissions with this control strategy (at least on the cooling design day). Finally, as mentioned above, the water flow rate per floor area is an important parameter for predicting SWT but not the hydronic HX rate. This is shown visually in Figure 10. Furthermore, since TABS extracts a higher heat gain rate than ESS-floor and TABS-insulation, the steady-state calculation results in higher water flow rates for TABS, and thus the reason why we see a higher number of test cases with TABS in bins above 0.003 $l \cdot s^{-1} \cdot m^{-2}$ in Figure 10. Figure 10 also shows that SWT does not increase significantly for flow rates higher than 0.006 $l \cdot s^{-1} \cdot m^{-2}$. Finally, Supplementary material 'c' contains additional visualizations comparing the impact of each parameter on SWT and the hydronic HX rate.

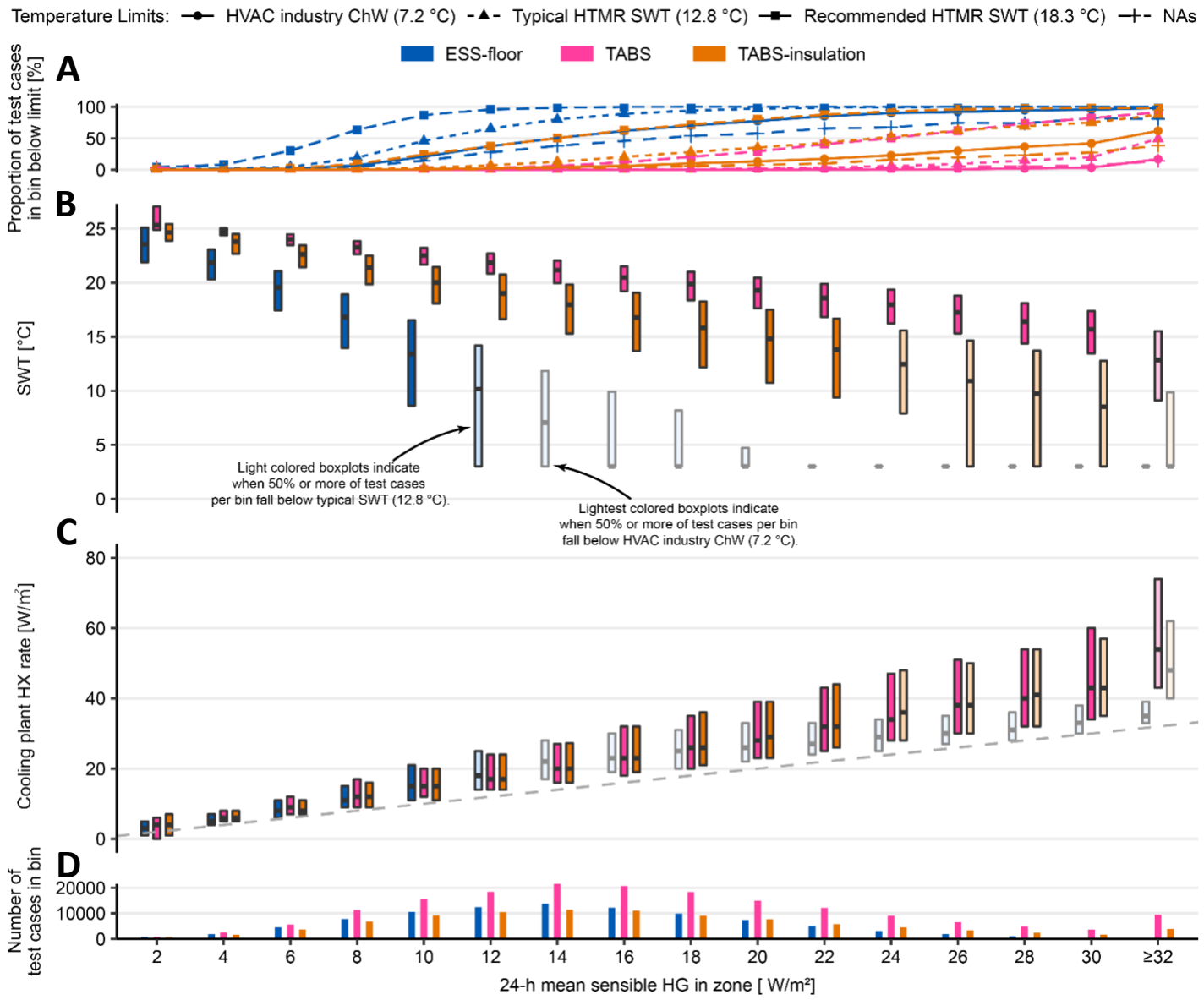

Figure 8: A) Proportion of test cases in each bin that are below the various temperature limits: HVAC industry ChW and typical and recommended minimum supply water temperatures (SWT) for high thermal mass radiant systems, B) SWT, C) cooling plant mean heat extraction (HX) rate during its operation duration, and D) number of test cases as a function of 24-hour mean sensible heat gain (HG) rate in zone expected to be extracted by the high thermal mass radiant system. The plots are binned up in 2-unit left-open intervals. The gray dashed lines in the C plots indicate where cooling plant HX is equal to HG metric. The boxplot become lighter colored when 50% or more of the test cases per bin fall below typical SWT (12.8 °C) and HVAC industry ChW (7.2 °C).

https://doi.org/10.1016/j.enbuild.2025.115387
escholarship.org/uc/item/3812p9p1

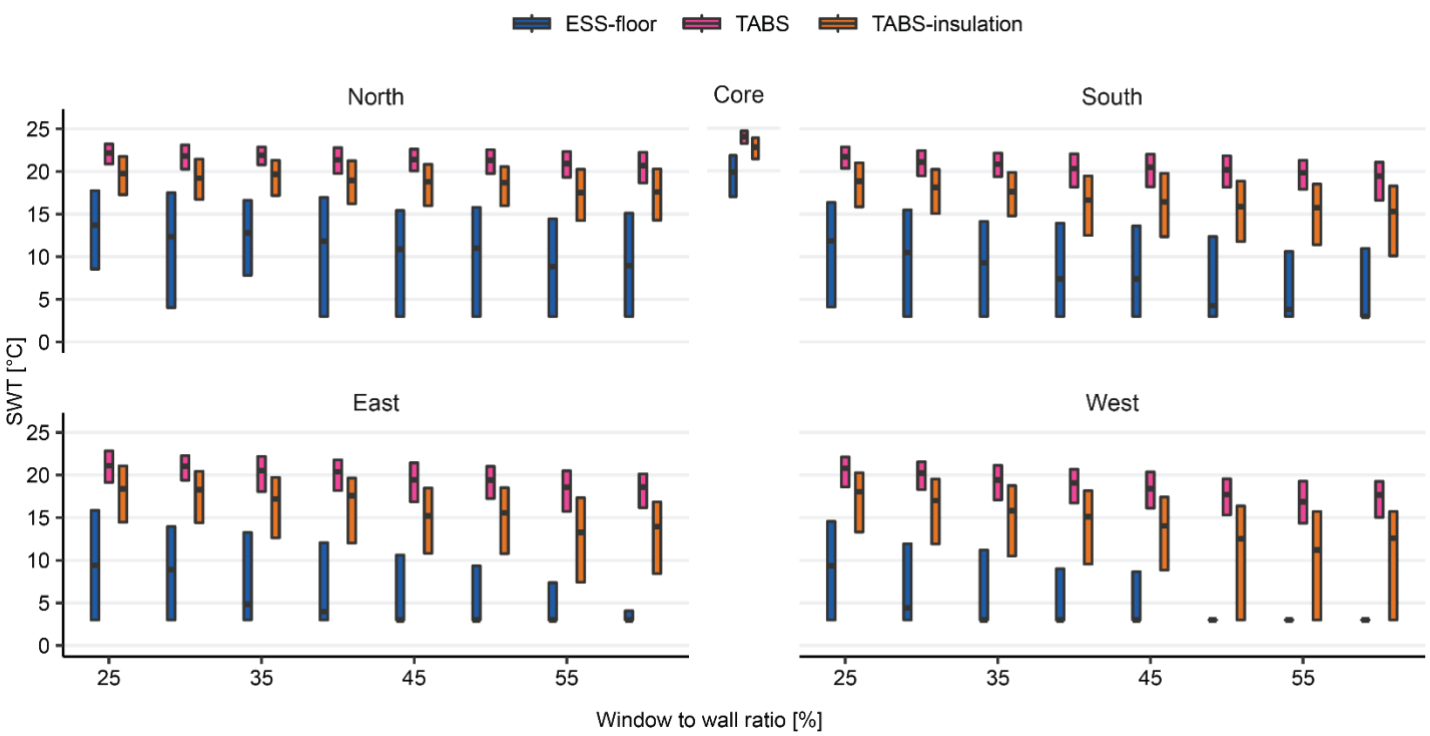

Figure 9: Supply water temperature (SWT) as a function of window-to-wall ratio, orientation, and radiant system type. The plots are binned up in 5-unit left-open intervals.

https://doi.org/10.1016/j.enbuild.2025.115387
escholarship.org/uc/item/3812p9p1

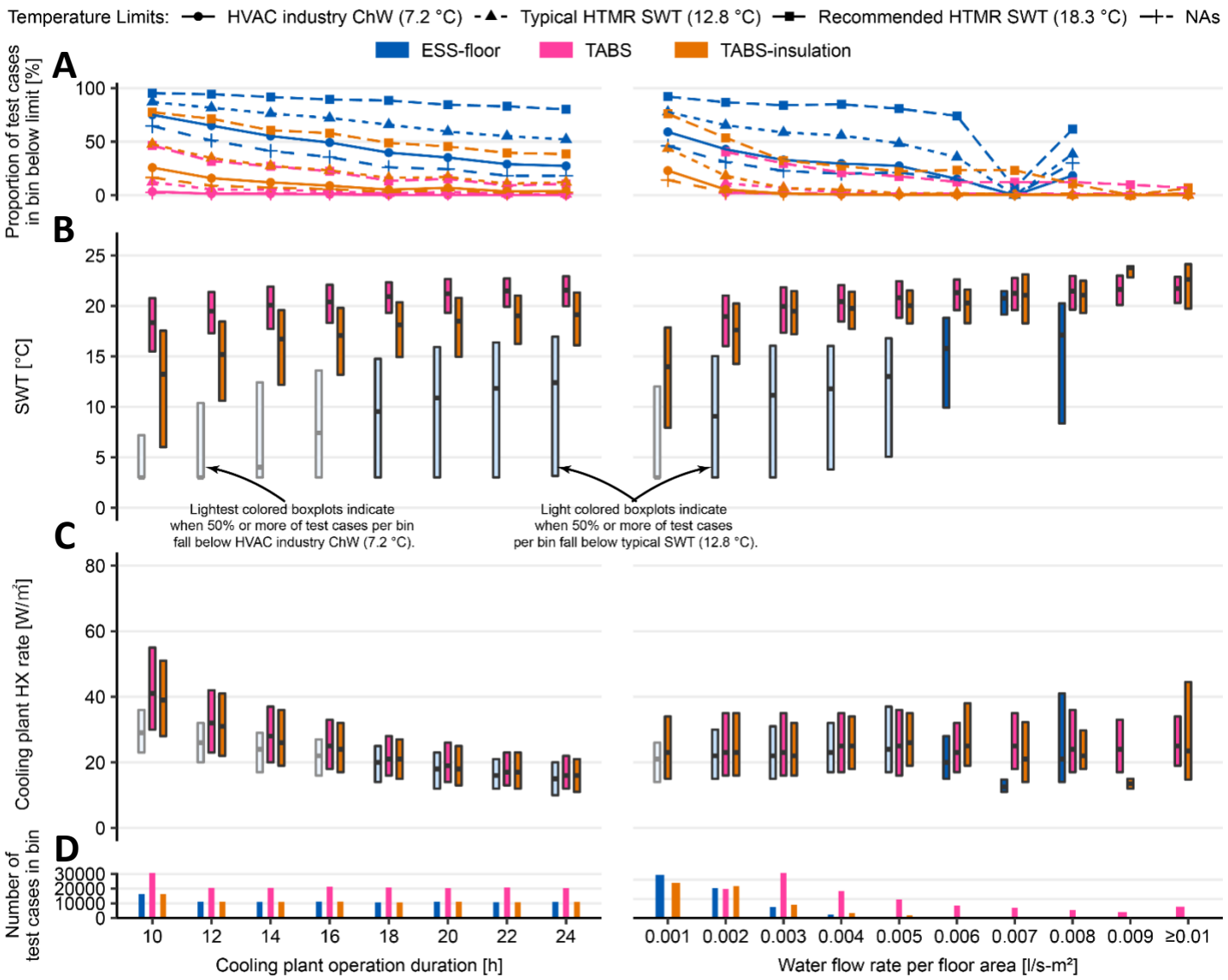

Figure 10: A) Proportion of test cases in each bin that are below the various temperature limits: HVAC industry ChW, typical, and recommended minimum supply water temperatures (SWT) for high thermal mass radiant systems, B) SWT, C) cooling plant mean heat extraction (HX) rate during its operation, D) number of test cases as a function of left) cooling plant operation duration and right) volumetric water flow rate per floor area. The plots are binned up in left) 2-unit and right) 0.001-unit left-open intervals. The boxplot become lighter colored when 50% or more of the test cases per bin fall below typical SWT (12.8 °C) and HVAC industry ChW (7.2 °C).

4. Discussion

HTMR can maintain comfortable temperatures at higher than typical SWT, and the cooling plant does not have to operate during the building's occupancy hours due to HTMR's capability to store thermal energy in the building's inherent thermal mass. These aspects provide an opportunity to integrate effective waterside economizing in an HTMR's cooling plant or completely replace the refrigeration cycle with adiabatic evaporative cooling for cooled water production. Our analysis shows that in 21 climate zones, it is possible to have for at least 40% of the operation hours the waterside economizing with a reasonable 4 °C approach temperature producing enough cooling. Building and radiant system designs capable of 100% waterside

https://doi.org/10.1016/j.enbuild.2025.115387
escholarship.org/uc/item/3812p9p1

economizing operation, i.e. no refrigeration cycle used, lie in the upper whiskers of the SWT distributions in Figure 6 for many climates and the upper portion of the IQR for some climate zones. This is especially true for core zones as seen in Figure 9. The SWT 25th percentile for core zones is greater than 19 °C. The potential to use only evaporative cooling increases if building designers can make two optimizations: 1) design their cooling plant in such a way that the HTMR operates during the night when wet-bulb temperatures are lower, and 2) design their building accordingly to reduce heat gains in the space. Figure 8 and the parameter importance analysis show a strong correlation between SWT and 24-hour mean heat gains expected to be removed by the HTMR. Thus, designers need to shift from using peak heat gains to 24-hour mean heat gains to design HTMR more effectively. For example, designers could maintain a 24-hour mean heat gain rate that is lower than 7, 14, and 24 W·m^{-2} for ESS-floor, TABS-insulation, and TABS, respectively, in order to achieve the recommended minimum SWT of 18.3 °C. ESS-floor has significantly lower capacity that it might not be a feasible high-temperature cooling system in many building applications. The main reason is due to the lower convective heat transfer coefficient for the floor surface when compared to the ceiling surface in cooling mode. Even though ESS-floor has only one active surface, its active surface radiatively cools all other exposed surfaces including the other passive ESS surface. This means there are greater thermal storage benefits when comparing to all-air systems. Peak heat gains are still important but primarily for designing the DOAS system and any supplemental cooling systems that outlier zones with high heat gains may require. In this study, no specific design measures have been taken to reduce loads such as shading, increased insulation, improved glazing, or reduced internal loads. More challenging climates will require design strategies that go beyond code requirements to use evaporative cooling successfully.

In Miami and Houston climates, where the wet bulb temperature is too high, cooling towers will not be very effective at producing the required SWT for cooling on the design day even if designers choose to operate the cooling plant at night and increase the performance of the cooling device. Yet, these climates benefit from using HTMR since the results in this study show that 50% of test cases for ESS-floor TABS, and TABS-insulation can use 0.5, 13.3, and 10 °C, respectively, warmer SWT than the typical 7.2 °C for all-air systems. A warmer SWT translates directly to increased central plant efficiency, since it reduces the effort to cool water, even when the refrigeration cycle is used (e.g. an air- or water-cooled chiller). A chiller's coefficient of performance (COP) during typical operation ranges from 3 to 7, and it can increase by up to 29% with the combination of warmer SWT and lower ambient temperatures by operating at night, i.e. low-lift operation (Gayeski, Armstrong, and Norford 2012; Seshadri, Rysanek, and Schlueter 2019). However, cooling towers operate at a fraction of the energy cost; COP range from 15 to 19 or even higher (Costelloe and Finn 2007) which is a significant improvement over the refrigeration cycle. Thus, there is a strong incentive to design chillers out of the cooling plant. Chiller lift is the temperature difference between the refrigerant's saturated condensing and saturated evaporating states. Building designers can reduce their system's lift by decreasing the entering condenser fluid temperature and increasing the chiller's SWT in which HTMR has a positive impact on both of these parameters.

Another major incentive is to avoid the capital cost of providing refrigeration capacity in the first place. In the US, chiller costs range from $375 to $8,875 per refrigeration ton, whereas it is $80 to $800 per equivalent refrigeration ton for cooling towers and fluid coolers (Gordian Group 2019). For context, the chiller cost is between $5 and $126 per square meter at a cooling load density of 50 W·m^{-2}. This is sufficiently high that avoiding that initial cost by using cooling tower plus radiant design is likely a much lower overall initial cost option than other more conventional radiant designs. Even if designing the chiller out of the cooling plant is unfeasible, HTMR can still reduce its design capacity up to 61% through an increased number of cooling plant

operation hours as seen in Figure 10. This also signifies that time is an important parameter in the HTMR cooling plant sizing procedure. Therefore, this leads to the conclusion that steady-state calculations are inadequate to properly size HTMR cooling plant.

There are other approaches to address cases where it is not feasible to further reduce design heat gains. Elevated airspeeds can provide occupant thermal comfort at higher indoor temperatures (Schiavon and Melikov 2008), which would increase the warmest SWT that will still provide a comfortable environment. The elevated airspeeds can also provide higher convective heat transfer with the active surfaces in the zone during both occupied and unoccupied hours (Pantelic et al. 2018; Karmann et al. 2018). This will accelerate the cooling of the building's thermal mass in preparation for the occupied period of the building.

Another consideration is that designers need to consider the proper control of the humidity during times when the ventilation system is typically turned off, especially in humid climates. Infiltration can increase the humidity levels in the zone, and an inactive ventilation system that does not control space humidity levels can lead to increased condensation risks in these climates. One option to mitigate this issue is to integrate an air recirculation mode so that the DOAS system can use 100% recirculation to more efficiently maintain space dewpoint conditions during unoccupied hours rather than running with 100% outside air.

Another aspect to consider is the control of the system outside of design day conditions. This paper performed simulations using only the cooling design day of each climate, and an annual simulation would have quite different results because the radiant system may either operate fewer hours, or may further increase the SWT, on less extreme days depending on the control strategy used. This likely means more opportunities for waterside economizing operation throughout much of the year, even in the more extreme climates. Raftery et al. (2017) presented a control strategy for HTMR that can account for different SWT and hours of operation. An analysis of the annual simulation for these models is out of scope for this current study but it's a natural follow-up study. The current study focuses on sizing considerations using design day scenarios.

When comparing the results of this study to the ISO standard 11855-2012 procedure, we observed that ISO standard generally underestimates the total heat extraction energy for HTMR. Using the standard 11855-2012 procedure will obscure considerable opportunities to reduce costs and improve energy efficiency and thermal comfort. In this study, we account for a wide range of building and radiant system characteristics to show building designers the impact of 27 parameters on the SWT and the cooling plant mean heat extraction rate during its operation. Our simulations include the time of day that HTMR operation occurs, which has a strong impact on the range of temperatures that occur in the space during occupied hours. Our simulations also account for shortwave radiation on surfaces including on the active surfaces which has a significant impact on its surface heat extraction rate. Therefore, we recommend HTMR designers to calculate the system's water flow rate using Equation 5 derived from this study's simulation results.

$$\hat{\dot{V}}_{area} = 0.00023\overline{HG}_{\Delta T} \qquad \text{Equation 5}$$

Where $\hat{\dot{V}}_{area}$ is volumetric water flow rate per floor area in $l \cdot s^{-1} \cdot m^{-2}$ and $\overline{HG}_{\Delta T}$ is the 24-hour mean sensible heat gains divided by the supply/return temperature difference. Equation 5 applies where ΔR_{X-G} is greater

than or equal to 0 but less than or equal to 1. Designers can then refer to Figure 8 to estimate the range for the required SWT and the cooling plant mean heat extraction rate for the expected 24-hour mean sensible heat gain rate in their zone. Designers should avoid going over 24-hour mean sensible heat gain rates where this study's results shows that 50% or more of the test cases per bin fall below typical SWT (12.8 °C) i.e. 10, 22, and 30 $W \cdot m^{-2}$ for ESS-floor, TABS-insulation, and TABS, respectively. The next important parameter that designers need to consider is HTMR's operation duration. The longer the HTMR's operation, the higher the SWT and the lower that the cooling plant mean heat extraction rate can be. However, we recommend operating the HTMR between 12-18 hours. The HTMR system can still avoid unfavorable operating conditions, e.g. high electricity prices or extreme weather conditions, when using the recommended operation interval duration while still taking advantage of reduced cooling plant sizes.

Finally, HTMR is mostly only practical for new construction, especially TABS. ESS systems can be used in some retrofit applications, but designers must consider the limited capacity of these systems. In this study, ESS-floor resulted in a median 24-hour mean surface HX rate of 13 $W \cdot m^{-2}$ which is 13% less than TABS. However, it can improve by reducing the SWT. Including ESS-floor in a retrofit is likely unfeasible unless a building's envelope is also retrofitted to reduce the design heat gains to a sufficiently low level to make ESS-floor effective at controlling indoor air temperatures and still benefit from high-temperature cooling. Another limitation is the added weight that the addition of a radiant layer would have on the building's structure.

5. Conclusion

We investigated the warmest supply water temperature (SWT) that can be used in high thermal mass radiant systems (HTMR) for cooling while maintaining comfortable temperatures. The models represent ASHRAE 90.1-2016 and Title 24-2016 code-compliant buildings in 14 US and 16 California climate zones. We found that resulting SWT of 12.3, 18.2, and 21.1 °C for the first quartile, median, and third quartile, respectively, among all test cases. These higher than typical SWT open the possibility to use adiabatic evaporative cooling devices such as cooling towers and fluid coolers combined with HTMR to increase waterside economizing operation in the cooling plant and, in some cases, eliminate the refrigeration cycle from the primary cooling system. It is easier to achieve high-temperature cooling with HTMR that has two active surfaces, i.e. TABS, since it can use SWT that is at least 4 °C warmer and can increase the peak active surface HX rate by at least 2 $W \cdot m^{-2}$ compared to HTMR with only one active surface, i.e. ESS-floor and TABS-insulation. ESS-floor that has the floor as the active surface requires significantly lower SWT than TABS and TABS-insulation. For this reason, TABS and TABS-insulation are the recommended HTMR installation for new construction. ESS-floor can be done for retrofits but has many limitations.

Our analysis shows that in 21 climate zones, it is possible to have for at least 40% of the operation hours the waterside economizing with a reasonable 4 °C approach temperature producing enough cooling. Waterside economizing operation can increase by minimizing heat gains entering and generating inside the zone, shifting the cooling plant's operation to nighttime hours when ambient temperatures are the lowest, and allowing the cooling plant to operate for a larger fraction in a 24-hour period. To properly design HTMR, building designers must use the 24-hour mean heat gain rate instead of the peak heat gain rate to size the cooling plant. Specifically, designers should maintain a 24-hour mean heat gain rate that is lower than 7, 14, and 24 $W \cdot m^{-2}$ for ESS-floor, TABS-insulation, and TABS, respectively, in order to achieve the recommended minimum SWT of 18.3 °C. Building designers must also consider time as an important sizing parameter which means that steady-state design calculations are inadequate for the proper design of HTMR.

6. Acknowledgment

This work was supported by the California Energy Commission (CEC) Electric Program Investment Charge (EPIC) under Contract EPC-14-009, “Optimizing Radiant Systems for Energy Efficiency and Comfort”, and the Center for the Built Environment, UC Berkeley, California.

7. References

Arens, Edward, Tyler Hoyt, Xin Zhou, Li Huang, Hui Zhang, and Stefano Schiavon. 2015. “Modeling the Comfort Effects of Short-Wave Solar Radiation Indoors.” *Building and Environment*, Interactions between human and building environment, 88:3–9. https://doi.org/10.1016/j.buildenv.2014.09.004.

ASHRAE. 2016. *ASHRAE Standard 90.1-Energy Standard for Buildings except Low-Rise Residential Buildings*. Atlanta, GA: American Society of Heating, Refrigerating and Air Conditioning Engineers, Inc. https://www.ashrae.org/resources--publications/bookstore/standard-90-1.

———. 2017. *2017 ASHRAE Handbook: Fundamentals*. Atlanta, GA: American Society of Heating, Refrigerating and Air-Conditioning Engineers.

———. 2020. “Chapter 6: Radiant Heating and Cooling.” In *HVAC Systems and Equipment*. Atlanta, GA: American Society of Heating, Refrigerating and Air Conditioning Engineers.

ASTM. 2017. “ASTM F876:2017 - Standard Specification for Crosslinked Polyethylene (PEX) Tubing.” https://compass.astm.org/download/F876.25806.pdf.

Bell, Ian H., Jorrit Wronski, Sylvain Quoilin, and Vincent Lemort. 2014. “Pure and Pseudo-Pure Fluid Thermophysical Property Evaluation and the Open-Source Thermophysical Property Library CoolProp.” *Industrial & Engineering Chemistry Research* 53 (6): 2498–2508. https://doi.org/10.1021/ie4033999.

Burhenne, Sebastian, Dirk Jacob, and Gregor P. Henze. 2011. “Sampling Based on Sobol’ Sequences for Monte Carlo Techniques Applied to Building Simulations.” In *12th Conference of International Building Performance Simulation Association*, 1816–23. Sydney Australia: International Building Performance Simulation Association.

CEC. 2015. “Title-24 2016 Part 6: Building Energy Efficiency Standards for Residential and Nonresidential Buildings.” In *Title 24 of the California Code of Regulations*. Sacramento, CA: California Energy Commission. https://ww2.energy.ca.gov/2015publications/CEC-400-2015-037/CEC-400-2015-037-CMF.pdf.

———. 2016. *2016 Nonresidential Alternative Calculation Method Reference Manual*. Sacramento, CA: California Energy Commission. https://energycodeace.com/site/custom/public/reference-ace-2016/index.html#!Documents/11purpose1.htm.

Chantrasrisalai, Chanvit, Vinay Ghatti, Daniel E. Fisher, and David G. Scheatzle. 2003. “Experimental Validation of the EnergyPlus Low-Temperature Radiant Simulation.” *ASHRAE Transactions* 109 (2): 614–23.

Chen, Xue-wen, and Jong Cheol Jeong. 2007. “Enhanced Recursive Feature Elimination.” In *Sixth International Conference on Machine Learning and Applications*, 429–35. Cincinnati, OH: IEEE. https://doi.org/10.1109/ICMLA.2007.35.

Costelloe, B, and D Finn. 2003. “Experimental Energy Performance of Open Cooling Towers Used under Low and Variable Approach Conditions for Indirect Evaporative Cooling in Buildings.” *Building Services Engineering Research and Technology* 24 (3): 163–77. https://doi.org/10.1191/0143624403bt069oa.

Costelloe, B., and D. Finn. 2007. “Thermal Effectiveness Characteristics of Low Approach Indirect Evaporative Cooling Systems in Buildings.” *Energy and Buildings* 39 (12): 1235–43. https://doi.org/10.1016/j.enbuild.2007.01.003.

Dawe, Megan, Paul Raftery, Jonathan Woolley, Stefano Schiavon, and Fred Bauman. 2020. “Comparison of Mean Radiant and Air Temperatures in Mechanically-Conditioned Commercial Buildings from over 200,000 Field and Laboratory Measurements.” *Energy and Buildings* 206:109582. https://doi.org/10.1016/j.enbuild.2019.109582.

Dean, Brian, John Dulac, Trevor Morgan, and Uwe Remme. 2018. “The Future of Cooling: Opportunities for Energy Efficient Air Conditioning.” IEA.

Deru, Michael, Kristin Field, Daniel Studer, Kyle Benne, Brent Griffith, Paul Torcellini, Bing Liu, et al. 2011. “U.S. Department of Energy Commercial Reference Building Models of the National Building Stock.” Technical Report. National Renewable Energy Laboratory.

DOE. 2018. “Weather Data | EnergyPlus.” Weather Data. 2018. https://energyplus.net/weather.

Duarte, Carlos, Paul Raftery, Stefano Schiavon, and Fred Bauman. 2018. “How High Can You Go? Determining the Highest Supply Water Temperature for High Thermal Mass Radiant Cooling Systems in California.” In *Proceedings of the 4th International Conference On Building Energy & Environment 2018*, 585–90. Melbourne, Australia. https://escholarship.org/uc/item/0s06q03g.

Duarte, Carlos, Kevin Van Den Wymelenberg, and Craig Rieger. 2013. “Revealing Occupancy Patterns in an Office Building through the Use of Occupancy Sensor Data.” *Energy and Buildings* 67 (December):587–95. https://doi.org/10.1016/j.enbuild.2013.08.062.

EIA. 2022. “Commercial Buildings Energy Consumption Survey (CBECS) Data.” Energy Information Administration, U.S. Department of Energy. https://www.eia.gov/consumption/commercial/data/2018/index.php?view=characteristics.

Friedman, Jerome H. 2002. “Stochastic Gradient Boosting.” *Computational Statistics & Data Analysis*, Nonlinear Methods and Data Mining, 38 (4): 367–78. https://doi.org/10.1016/S0167-9473(01)00065-2.

Gayeski, N. T., P. R. Armstrong, and L. K. Norford. 2012. “Predictive Pre-Cooling of Thermo-Active Building Systems with Low-Lift Chillers.” *HVAC&R Research* 18 (5): 858–73. https://doi.org/10.1080/10789669.2012.643752.

Gordian Group. 2019. *Mechanical Costs With RSmeans Data 2020*. Edited by Joseph Kelble. 43rd Annual edition. Gordian Group Inc RSMeans.

Higgins, Cathy, and Kevin Carbonnier. 2017. “Energy Performance of Commercial Buildings with Radiant Heating and Cooling.” https://escholarship.org/uc/item/34f0h35q.

Isaac, Morna, and Detlef P. van Vuuren. 2009. “Modeling Global Residential Sector Energy Demand for Heating and Air Conditioning in the Context of Climate Change.” *Energy Policy* 37 (2): 507–21. https://doi.org/10.1016/j.enpol.2008.09.051.

ISO. 2012. *ISO 11855:2012 - Building Environment Design-Design, Dimensioning, Installation and Control of Embedded Radiant Heating and Cooling Systems*. Geneva, Switzerland: International Organization for Standardization. http://www.iso.org/iso/iso_catalogue/catalogue_tc/catalogue_detail.htm?csnumber=52408.

IWBI. 2021. “WELL Building Standard V2.” New York, NY: International WELL Building Institute. https://v2.wellcertified.com/v2.2/en/overview.

Joe, Stephen, and Frances Y. Kuo. 2008. “Constructing Sobol Sequences with Better Two-Dimensional Projections.” *SIAM Journal on Scientific Computing* 30 (5): 2635–54. https://doi.org/10.1137/070709359.

Karmann, Caroline, Fred Bauman, Paul Raftery, Stefano Schiavon, and Mike Koupriyanov. 2018. “Effect of Acoustical Clouds Coverage and Air Movement on Radiant Chilled Ceiling Cooling Capacity.” *Energy and Buildings* 158 (January):939–49. https://doi.org/10.1016/j.enbuild.2017.10.046.

Karmann, Caroline, Stefano Schiavon, and Fred Bauman. 2017. “Thermal Comfort in Buildings Using Radiant vs. All-Air Systems: A Critical Literature Review.” *Building and Environment* 111 (Supplement C): 123–31. https://doi.org/10.1016/j.buildenv.2016.10.020.

Karmann, Caroline, Stefano Schiavon, Lindsay T. Graham, Paul Raftery, and Fred Bauman. 2017. “Comparing Temperature and Acoustic Satisfaction in 60 Radiant and All-Air Buildings.” *Building and Environment* 126 (December):431–41. https://doi.org/10.1016/j.buildenv.2017.10.024.

Kuhn, Max. 2008. “Building Predictive Models in R Using the Caret Package.” *Journal of Statistical Software* 28 (5). https://doi.org/10.18637/jss.v028.i05.

La, D., Y. J. Dai, Y. Li, R. Z. Wang, and T. S. Ge. 2010. “Technical Development of Rotary Desiccant Dehumidification and Air Conditioning: A Review.” *Renewable and Sustainable Energy Reviews* 14 (1): 130–47. https://doi.org/10.1016/j.rser.2009.07.016.

Lehmann, Beat, Viktor Dorer, and Markus Koschenz. 2007. “Application Range of Thermally Activated Building Systems Tabs.” *Energy and Buildings* 39 (5): 593–98. https://doi.org/10.1016/j.enbuild.2006.09.009.

Li, Jiayu, Jovan Pantelic, Coleman B. Merchant, Kian Wee Chen, Ippei Izuhara, Ryosuke Yuki, Forrest M Meggers, and Stefano Schiavon. 2024. “Comparison of the Environmental, Energy, and Thermal Comfort Performance of Air and Radiant Cooling Systems in a Zero-Energy Office Building in Singapore.” *Energy and Buildings* 318 (September):114487. https://doi.org/10.1016/j.enbuild.2024.114487.

Mahmood, Muhammad H., Muhammad Sultan, Takahiko Miyazaki, Shigeru Koyama, and Valeriy S. Maisotsenko. 2016. “Overview of the Maisotsenko Cycle – A Way towards Dew Point Evaporative Cooling.” *Renewable and Sustainable Energy Reviews* 66 (December):537–55. https://doi.org/10.1016/j.rser.2016.08.022.

Meierhans, R. A. 1996. “Room Air Conditioning by Means of Overnight Cooling of the Concrete Ceiling.” *ASHRAE Transactions* 102 (1): 693–97.

Ning, Baisong, Stefano Schiavon, and Fred S. Bauman. 2017. “A Novel Classification Scheme for Design and Control of Radiant System Based on Thermal Response Time.” *Energy and Buildings* 137 (February):38–45. https://doi.org/10.1016/j.enbuild.2016.12.013.

Niu, J. L., J. V. D. Kooi, and H. V. D. Rhee. 1995. “Energy Saving Possibilities with Cooled-Ceiling Systems.” *Energy and Buildings* 23 (2): 147–58. https://doi.org/10.1016/0378-7788(95)00937-X.

Niu, J. L., L. Z. Zhang, and H. G. Zuo. 2002. “Energy Savings Potential of Chilled-Ceiling Combined with Desiccant Cooling in Hot and Humid Climates.” *Energy and Buildings* 34 (5): 487–95. https://doi.org/10.1016/S0378-7788(01)00132-3.

Olesen, Bjarne W., and Günther Zöllner. 2007. “New European Standards for Design, Dimensioning and Testing Embedded Radiant Heating and Cooling Systems.” *Proceedings of Clima 2007 WellBeing Indoors*. https://www.irbnet.de/daten/iconda/CIB8359.pdf.

Paliaga, Gwelen, Farhad Farahmand, Paul Raftery, and Jonathan Woolley. 2017. “TABS Radiant Cooling Design & Control in North America: Results from Expert Interviews.” *eScholarship*, June. http://escholarship.org/uc/item/0w62k5pq.

Pantelic, Jovan, Stefano Schiavon, Baisong Ning, Eleftherios Burdakis, Paul Raftery, and Fred Bauman. 2018. “Full Scale Laboratory Experiment on the Cooling Capacity of a Radiant Floor System.” *Energy and Buildings* 170 (July):134–44. https://doi.org/10.1016/j.enbuild.2018.03.002.

Philip, Santosh. 2016. “Eppy.” https://pypi.python.org/pypi/eppy/0.5.2.

Raftery, Paul, Carlos Duarte, Stefano Schiavon, and Fred Bauman. 2017. “A New Control Strategy for High Thermal Mass Radiant Systems.” In *Proceedings of Building Simulation 2017*. San Francisco, CA: International Building Performance Simulation Association. http://escholarship.org/uc/item/5tz4n92b.

Raftery, Paul, Carlos Duarte Roa, Starr Yang, Stefano Schiavon, and Fred Bauman. 2019. “CBE Rad Tool.” Berkeley, CA: Center for the Built Environment, University of California Berkeley. http://radiant.cbe.berkeley.edu/.

Raftery, Paul, Kwang Ho Lee, Tom Webster, and Fred Bauman. 2012. “Performance Analysis of an Integrated UFAD and Radiant Hydronic Slab System.” *Applied Energy*, Energy Solutions for a Sustainable World, Special Issue of International Conference of Applied Energy, ICA2010, April 21-23, 2010, Singapore, 90 (1): 250–57. https://doi.org/10.1016/j.apenergy.2011.02.014.

Rhee, Kyu-Nam, and Kwang Woo Kim. 2015. “A 50 Year Review of Basic and Applied Research in Radiant Heating and Cooling Systems for the Built Environment.” *Building and Environment*, Fifty Year Anniversary for Building and Environment, 91 (September):166–90. https://doi.org/10.1016/j.buildenv.2015.03.040.

Saber, Esmail M., Kwok Wai Tham, and Hansjürg Leibundgut. 2016. “A Review of High Temperature Cooling Systems in Tropical Buildings.” *Building and Environment* 96 (February):237–49. https://doi.org/10.1016/j.buildenv.2015.11.029.

Saltelli, Andrea, Paola Annoni, Ivano Azzini, Francesca Campolongo, Marco Ratto, and Stefano Tarantola. 2010. “Variance Based Sensitivity Analysis of Model Output. Design and Estimator for the Total Sensitivity Index.” *Computer Physics Communications* 181 (2): 259–70. https://doi.org/10.1016/j.cpc.2009.09.018.

Samuel, D. G. Leo, S. M. Shiva Nagendra, and M. P. Maiya. 2013. “Passive Alternatives to Mechanical Air Conditioning of Building: A Review.” *Building and Environment* 66:54–64. https://doi.org/10.1016/j.buildenv.2013.04.016.

Schiavon, Stefano, and Arsen K. Melikov. 2008. “Energy Saving and Improved Comfort by Increased Air Movement.” *Energy and Buildings* 40 (10): 1954–60. https://doi.org/10.1016/j.enbuild.2008.05.001.

Seshadri, Bharath, Adam Rysanek, and Arno Schlueter. 2019. “High Efficiency ‘Low-Lift’ Vapour-Compression Chiller for High-Temperature Cooling Applications in Non-Residential Buildings in Hot-Humid Climates.” *Energy and Buildings* 187 (March):24–37. https://doi.org/10.1016/j.enbuild.2019.01.028.

Sobol, I. M. 1976. “Uniformly Distributed Sequences with an Additional Uniform Property.” *USSR Computational Mathematics and Mathematical Physics* 16 (5): 236–42. https://doi.org/10.1016/0041-5553(76)90154-3.

Sodec, Franc. 1999. “Economic Viability of Cooling Ceiling Systems.” *Energy and Buildings* 30 (2): 195–201. https://doi.org/10.1016/S0378-7788(98)00087-5.

Stetiu, Corina. 1999. “Energy and Peak Power Savings Potential of Radiant Cooling Systems in US Commercial Buildings.” *Energy and Buildings* 30 (2): 127–38. https://doi.org/10.1016/S0378-7788(98)00080-2.

Sverdlin, Boris, Alexey Tikhonov, and Ritta Gelfand. 2011. “Theoretical Possibility of The Maisotsenko Cycle Application to Decrease Cold Water Temperature in Cooling Towers.” *International Journal of Energy for a Clean Environment* 12 (2–4): 175–85. https://doi.org/10.1615/InterJEnerCleanEnv.2012005876.

Taylor, Steven T. 2011. “Optimizing Design & Control Of Chilled Water Plants: Part 3: Pipe Sizing and Optimizing Delta T.” *ASHRAE Journal*, December 2011.

———. 2014. “How to Design & Control Waterside Economizers.” *ASHRAE Journal* 56 (6): 30–36.

Tian, Zhen, and James A. Love. 2009. “Energy Performance Optimization of Radiant Slab Cooling Using Building Simulation and Field Measurements.” *Energy and Buildings* 41 (3): 320–30. https://doi.org/10.1016/j.enbuild.2008.10.002.

Tuaycharoen, N., and P. R. Tregenza. 2016. “View and Discomfort Glare from Windows:” *Lighting Research & Technology*, August. https://doi.org/10.1177/1365782807077193.

USGBC. 2020. “Leadership in Energy and Environmental Design.” Washington DC: US Green Building Council. http://www.usgbc.org/leed.

Wang, Xichun, Jianlei Niu, and A. H. C. van Paassen. 2008. “Raising Evaporative Cooling Potentials Using Combined Cooled Ceiling and MPCM Slurry Storage.” *Energy and Buildings* 40 (9): 1691–98. https://doi.org/10.1016/j.enbuild.2008.02.028.

Wickham, Hadley, Mara Averick, Jennifer Bryan, Winston Chang, Lucy McGowan, Romain François, Garrett Grolemund, et al. 2019. “Welcome to the Tidyverse.” *Journal of Open Source Software* 4 (43): 1686. https://doi.org/10.21105/joss.01686.

Zhang, L. Z. 2006. “Energy Performance of Independent Air Dehumidification Systems with Energy Recovery Measures.” *Energy* 31 (8): 1228–42. https://doi.org/10.1016/j.energy.2005.05.027.

Zhang, L. Z., and J. L. Niu. 2003. “Indoor Humidity Behaviors Associated with Decoupled Cooling in Hot and Humid Climates.” *Building and Environment* 38 (1): 99–107. https://doi.org/10.1016/S0360-1323(02)00018-5.

Zhou, Yuyu, Leon Clarke, Jiyong Eom, Page Kyle, Pralit Patel, Son H. Kim, James Dirks, et al. 2014. “Modeling the Effect of Climate Change on U.S. State-Level Buildings Energy Demands in an Integrated Assessment Framework.” *Applied Energy* 113 (January):1077–88. https://doi.org/10.1016/j.apenergy.2013.08.034.

Zhou, Yuyu, Jiyong Eom, and Leon Clarke. 2013. “The Effect of Global Climate Change, Population Distribution, and Climate Mitigation on Building Energy Use in the U.S. and China.” *Climatic Change* 119 (3–4): 979–92. https://doi.org/10.1007/s10584-013-0772-x.

Appendix

A. Details of two single simulations

Figure A-1 illustrates the timeseries results of the final outcome of the iterative process to find the warmest SWT for two examples cases that meet the given constraints and are similar to each other except in their location and control strategy. Figure A-1 A) shows the instantaneous sensible plus latent heat gain rate, B) heat extraction rates of various components, and C) the coincident outdoor and resulting indoor temperatures with a D) closeup of indoor temperatures during the cooling design day in left) Chicago, Illinois and right) Boise, Idaho. Table A-1 contains select design parameters and results for these two simulation cases.

Table A-1: Select design parameters and results for two example test case simulations.

Design parameter or result	Chicago	Boise
Radiant type	TABS-ceiling	TABS-ceiling
Supply water temperature	20.2 °C	18.7 °C
Peak hydronic heat extraction rate	38 W·m^{-2}	30 W·m^{-2}
Peak surfaces heat extraction rate	27 W·m^{-2}	35 W·m^{-2}
Simulated hydronic extracted energy	82 kWh	40 kWh
Estimated steady-state extracted energy (Q_{hyd})	201 kWh	95 kWh
Simulated sensible heat gain energy expected to be extracted by radiant system ($HG^{sen}_{sim_{zn}}$)	83 kWh	39 kWh
ΔR_{X-G}	0.59	0.59
Zone dimensions	7.5 x 35.5 m	6.6 x 17.5 m
Exterior wall orientation	25° (S)	31° (SW)
Window-to-wall ratio	34%	34%
Slab thickness	0.202 m	0.214 m
Tube spacing	0.2286 m	0.2286 m
Tube depth	0.094 m	0.129 m
Tube inside diameter	11.5 mm	16.4 mm
Number of tube circuit	24	8
Tube circuit length	51 m	107 m
Water flow rate per circuit	0.035 l·s^{-1}	0.043 l·s^{-1}
Water flow rate per area	0.00314 l·s^{-1}·m^{-2}	0.00188 l·s^{-1}·m^{-2}
Water flow rate-loop per area	0.0754 loop-l·s^{-1}·m^{-2}	0.0094 loop-l·s^{-1}·m^{-2}
Design temperature difference	5 °C	7 °C
Simulated temperature difference	1 °C	1.8 °C
Floor covering thermal resistance	0.113 K·m^2·W^{-1}	0.284 K·m^2·W^{-1}
Cooling plant starting time	21:00	0:00
Cooling plant operation duration	11 hours	15 hours

As mentioned in the methods section, the district cooling plant is sized to always provide the resulting SWT at each timestep of the cooling design day to operate as a constant temperature, constant flow rate system. Figure A-1 B) shows that the peak surface heat extraction rate can occur either when the hydronic plant is on or off. It all depends on the timing of the hydronic plant operation and the thermal response of the room. Radiation and convection heat gain rates through the windows and internal heat gain rates are the two dominant categories for these test cases. Figure A-1 A) shows all the sensible and latent heat gain rates relevant to the simulation model in which the sum of all these heat gain rates is referred to as the total heat gain rate of the zone. A portion of the total heat gain energy is extracted by the DOAS, another portion by the hydronic cooling plant, and the remaining is absorbed, stored, and released with a delay by the zone's thermal

mass back to the zone or the outdoor environment. The exact proportions depend on the capacities of the DOAS and hydronic cooling plant, the thermal response of the whole room, and the magnitude of the heat gain rate. For reference, the total simulated sensible heat gain ($HG_{sim_{zn}}^{sen}$) energy for the Chicago zone is 83 kWh and the estimated steady-state hydronic heat extraction (Q_{hyd}) energy is 201 kWh which results in 0.59 for ΔR_{X-G} in this test case. In the case for the Boise zone, the metrics are 39 kWh, 95 kWh, and 0.59 for $HG_{sim_{zn}}^{sen}$, Q_{hyd}, and ΔR_{X-G}, respectively. The test cases would lean towards the "SWT ≥ 18.3 °C" category. In these both cases, the simple rule of thumb using ΔR_{X-G} and

Figure 3 is in line with the SWT found through simulation.

The peak outdoor dry-bulb temperatures are 33 and 36.7 °C, for Chicago and Boise, respectively, and the indoor operative temperature during the occupied hours is maintained within the defined thermal comfort limits. The operative temperature rises throughout the occupied hours as heat is stored in the thermal mass of the zone, including the floor and ceiling surfaces of the building structure slab. As expected, the ceiling surface is colder than the floor surface since the tubing is closer to this active surface. The indoor dry-bulb air and mean radiant temperature closely follow the operative temperature which also implies that there is not a significant difference between them (Dawe et al. 2020). The SWT is marginally above the indoor dewpoint temperature for Chicago and clearly above for Boise which is important to reduce condensation risks in the space.

In summary, the most important takeaway from these visualizations is that the high thermal mass radiant system's operation and its disturbances are not steady-state and will not reach a steady-state condition. This is due to the high thermal inertia contain within the system and zone thermal dynamics. However, these aspects allow the hydronic plant to operate at anytime of day while the surface heat extraction rate responds to the incoming heat gains proportionally.

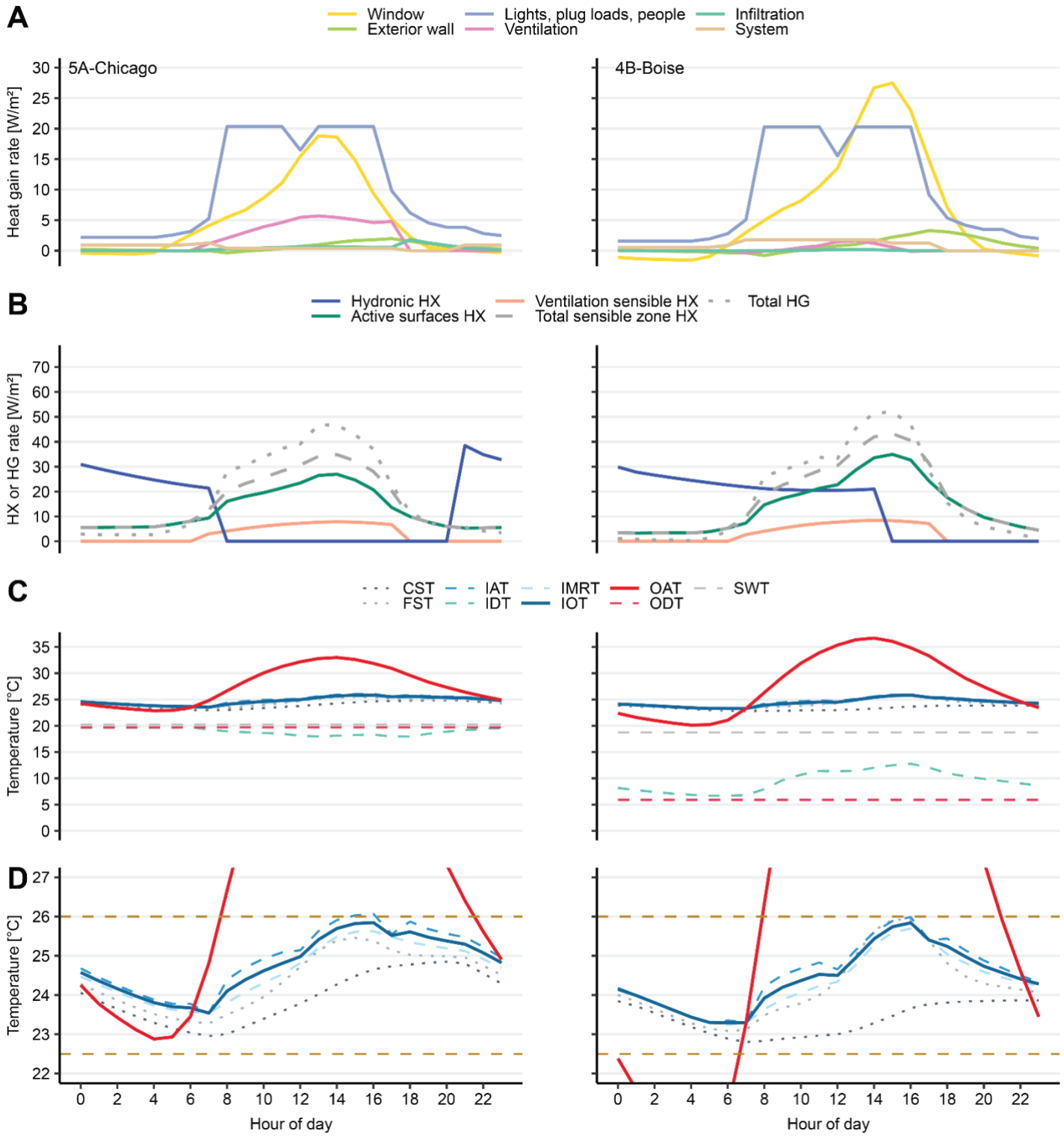

Figure A-1: Final outcome of the iterative process to find the warmest supply water temperature (SWT) that will maintain comfortable temperatures in the zone. This test case represents one good practical example of a building with TABS in Boise, ID. The resulting SWT for this case is 18.7 °C. A) shows the instantaneous total (sensible plus latent) heat gain (HG) rate and B) heat extraction (HX) rates of various components, and C) the coincident outdoor dry-bulb air (OAT) and dewpoint (ODT) and resulting

https://doi.org/10.1016/j.enbuild.2025.115387
escholarship.org/uc/item/3812p9p1

indoor operative (IOT), dry-bulb air (IAT), mean radiant (IMRT), dewpoint (IDT), ceiling (CST) and floor surface (FST), and SWT temperatures with a D) closeup of indoor temperatures during the cooling design day.

Supplementary material

a. Identifying NA and low supply water temperature in test cases

We created 360,900 test cases that we simulated on the cooling design day. After the simulation, we removed test cases from the main analysis where condensation issues in the space occurred. Condensation issues occur when the SWT is below the space's dew point temperature. In practice, chillers for all-air systems are designed to generate about 7.2 °C water temperatures thus using lower SWT for high thermal mass radiant (HTMR) systems is unreasonable, and a HTMR radiant system would not be selected as a viable design option in this case. Thus, we also note the number of test cases where peak design operative temperature was not reached, SWT is below 7.2 °C, and cooling is not needed. In total, we removed 4,952 where condensation issues occurred. The following list provides more details on how many test cases belong to each category that would not be implemented in practice. The percentages are taken from the total number of test cases we initially created.

1. 4,952 (1.4%) test cases due to condensation occurrences.
2. 38,716 (10.7%) test cases did not meet peak design operative temperature.
3. 17,486 (4.8%) test cases with SWT below 7.2 °C but met peak design operative temperature.
4. 517 (.14%) test cases above 26.25 °C and do not need cooling on the cooling design day.

In total, the four categories represent 17% of the results. Most cases in these categories are simulations where the iterative process adjusted below the minimum plant loop temperature limit (3 °C) without reaching the peak design operative temperature (e.g. zone was too warm) and SWT below 7.2 °C. The third highest number of test cases are due to condensation issues, and these were removed from the main analysis. Miami accounted for the most simulations (2,938) with condensation issues. It is no surprise since its wet-bulb temperature during the peak dry-bulb temperature on the cooling design day is 25.3 °C. Houston and Chicago had 678 and 426 simulations with condensation issues, respectively. Duluth, Minneapolis, Baltimore, Atlanta, and Seattle had a range of 266 to 56 simulations, and Fairbanks, 03-Oakland, and 08-Fullerton had less than 13 simulations. The rest of the US cities' climates had no condensation issues in the simulation.

Figure a-1 (A) shows that most of the condensation issues are during the hours when the DOAS system is turned off i.e. during unoccupied hours of the zone indicating the limitations of running HTMR outside occupied hours without proper humidity control. Furthermore, Figure a-1 (B) shows that this is especially true for climates with a design day dew point temperature of 17 °C or higher.

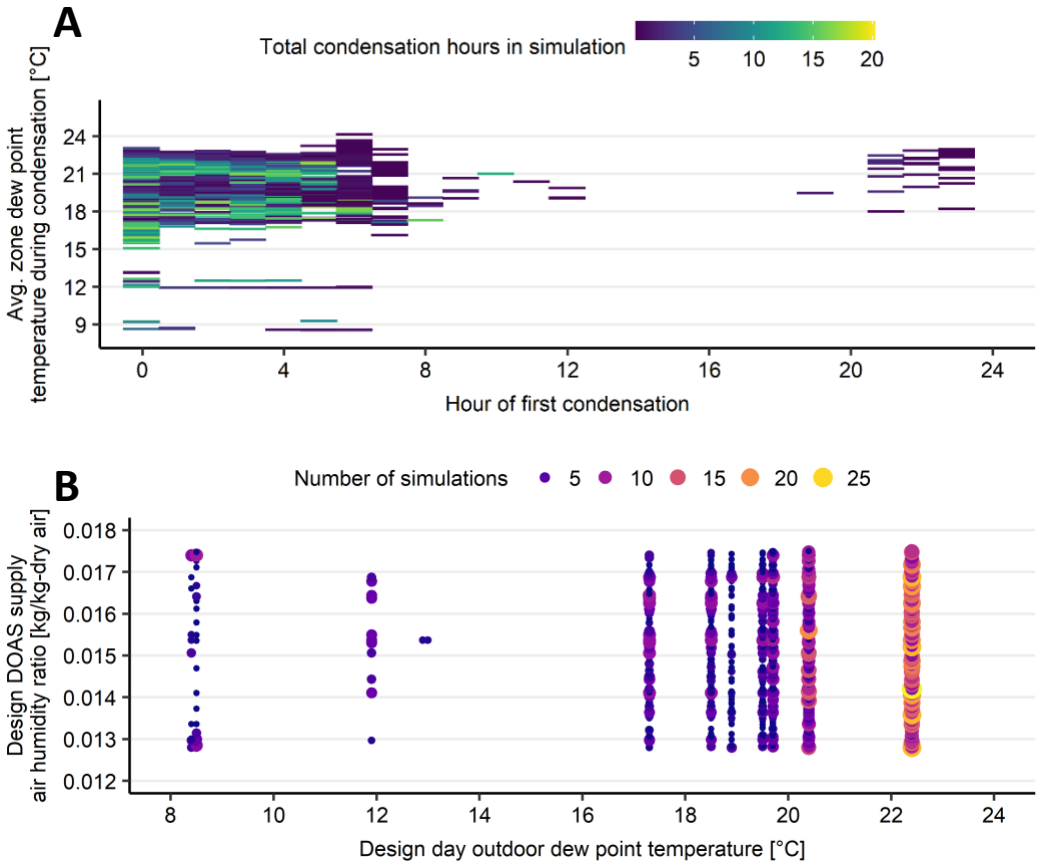

Figure a-1: Simulation test cases where condensation occurred for at least one hour. A) Hour at which the first condensation occurred in the simulation and the resulting dew point temperature for all hours of condensation and B) design dedicated outdoor air system (DOAS) supply air humidity ratio as a function of design day outdoor wet-bulb temperature.

a1. Carpet layer modeling technique

The number of removed test cases would have been higher if we had not changed the modeling technique in EnergyPlus for the carpet layer. We originally defined the carpet layer as a "no mass" object but many simulations were failing when EnergyPlus was calculating the conduction transfer function series. Most of the failing simulation cases had the embedded surface system (ESS) with the carpet layer. We fixed this issue by redefining the carpet layer as a full material definition that includes mass and other thermophysical properties. Thus, we recommend not to use the "no mass" material object simplification when defining the radiant system layers in EnergyPlus.

b. Heat gain rate estimate assumptions

We calculated heat gain rates for solar, internal, envelope, ventilation, and infiltration according to ASHRAE's 2017 Handbook of Fundamentals (ASHRAE 2017) to obtain heat gain rate estimates to feed into Duarte et al.'s (2018) random forest models. We assumed an average adult's skin surface area (DuBois area = 1.8 m^2) and 1.2 MET to find the instantaneous heat gain rate for occupants. We used the upper comfort limit as the indoor design condition for the space. For the outdoor design conditions, we used the 0.4% dry-bulb temperature and mean coincident wet-bulb temperature design day for each climate. We used cooling design day for the steady-state heat gain rate estimation as we did for the transient simulation in EnergyPlus. For the latent heat gain rate, we calculated the humidity difference between the model's design day condition and the sampled

DOAS design humidity ratio. We assumed latent heat of evaporation for water at 2,260 $kJ \cdot kg^{-1}$. We used the Python CoolProp package to calculate air properties at each climate's design day, i.e. specific heat, density, and humidity ratio (Bell et al. 2014). We followed ASHRAE's clear-sky solar calculation method to obtain the total solar radiation based on each model's location and orientation (ASHRAE 2017).

https://doi.org/10.1016/j.enbuild.2025.115387
escholarship.org/uc/item/3812p9p1

c. Effects from various building and radiant system design parameters

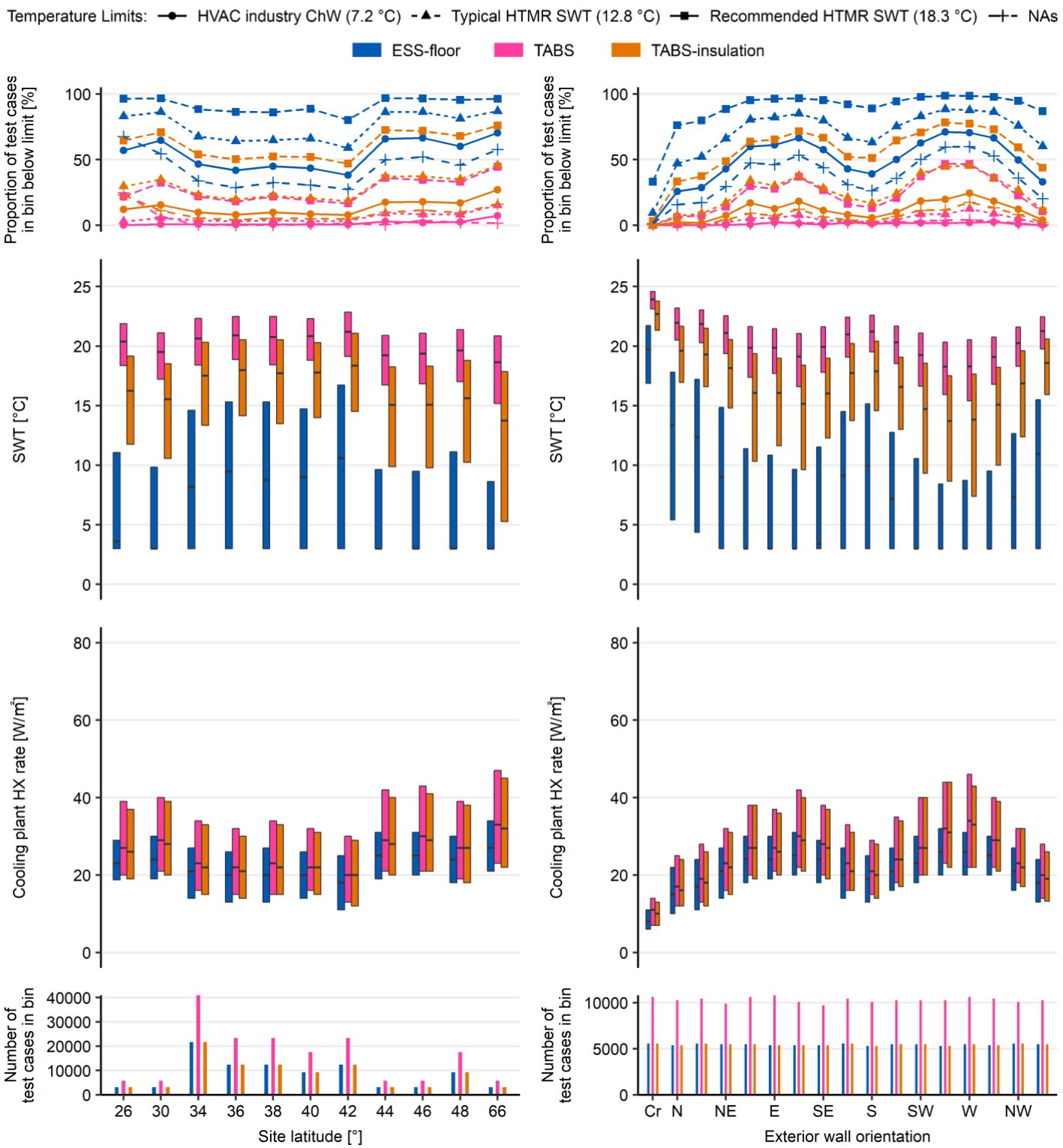

https://doi.org/10.1016/j.enbuild.2025.115387
escholarship.org/uc/item/3812p9p1

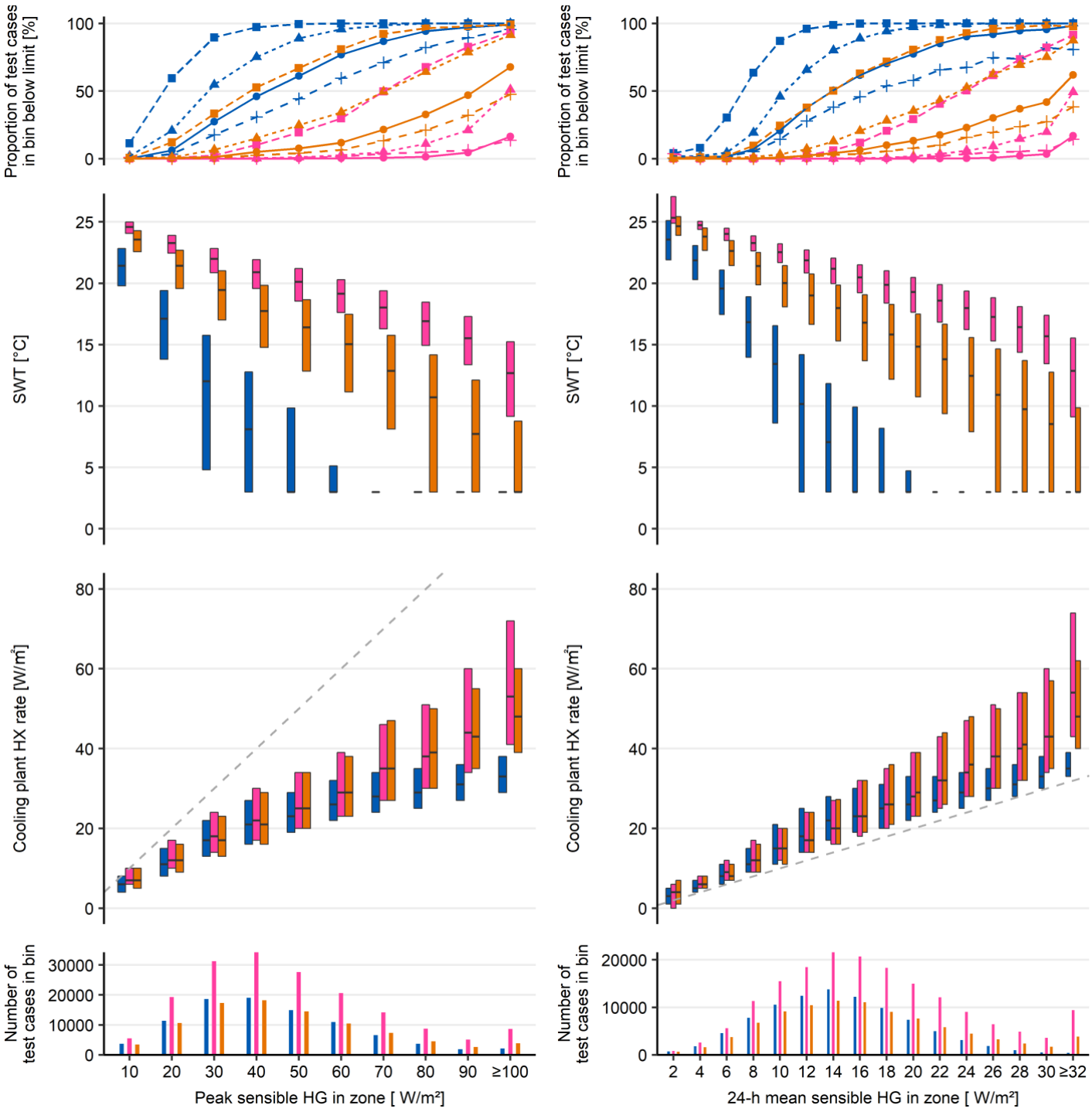

https://doi.org/10.1016/j.enbuild.2025.115387
escholarship.org/uc/item/3812p9p1

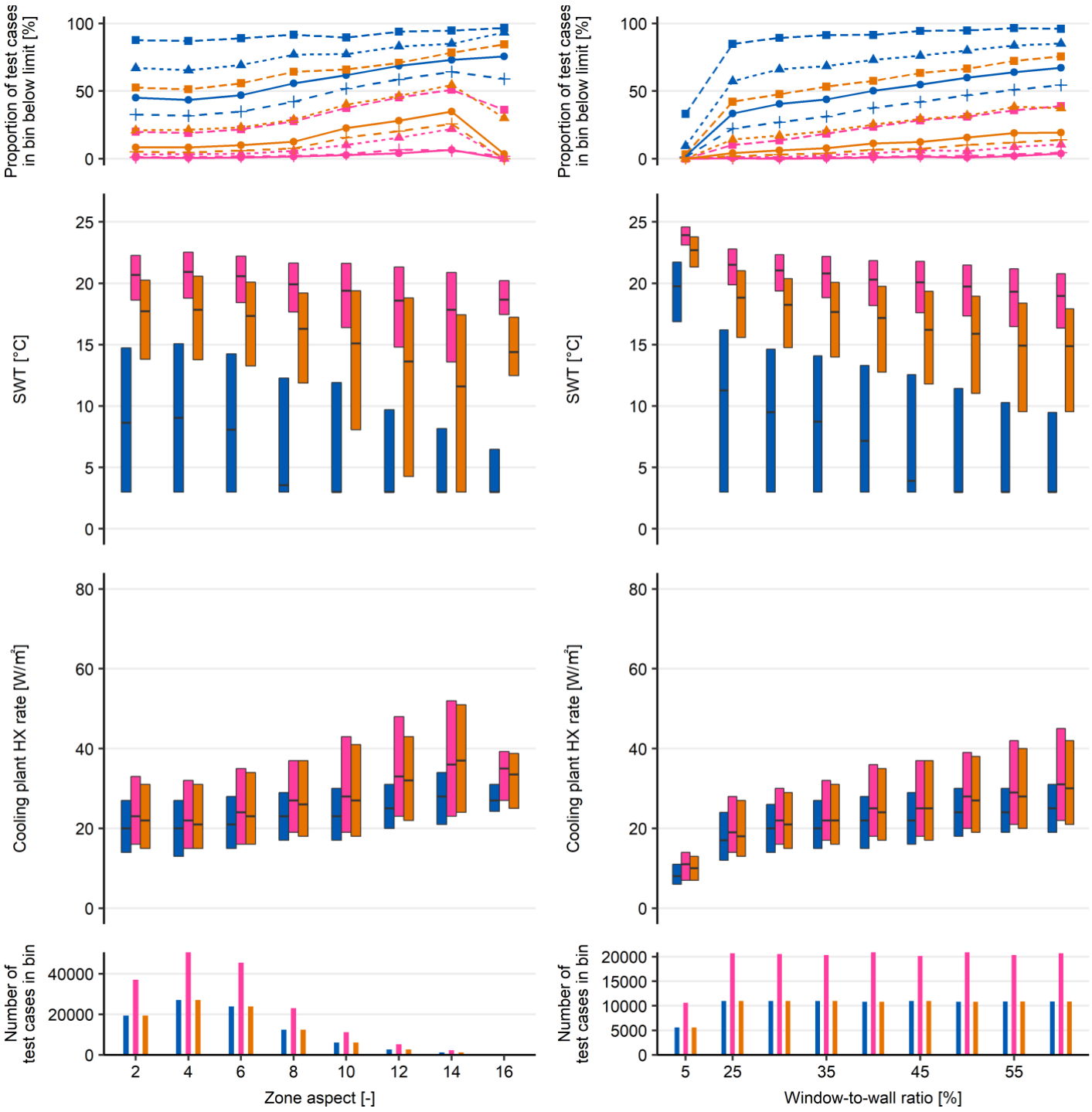

https://doi.org/10.1016/j.enbuild.2025.115387
escholarship.org/uc/item/3812p9p1

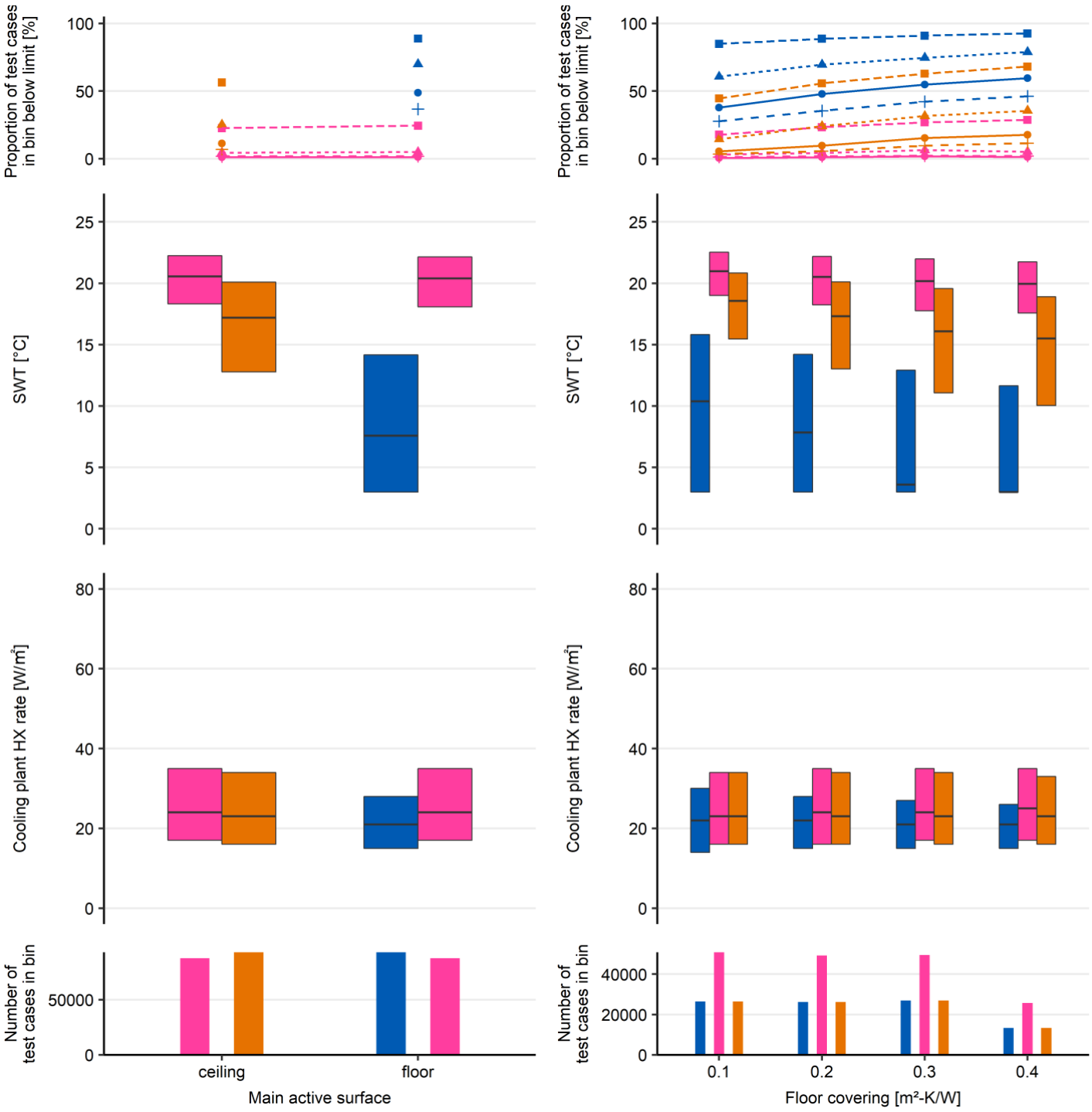

https://doi.org/10.1016/j.enbuild.2025.115387
escholarship.org/uc/item/3812p9p1

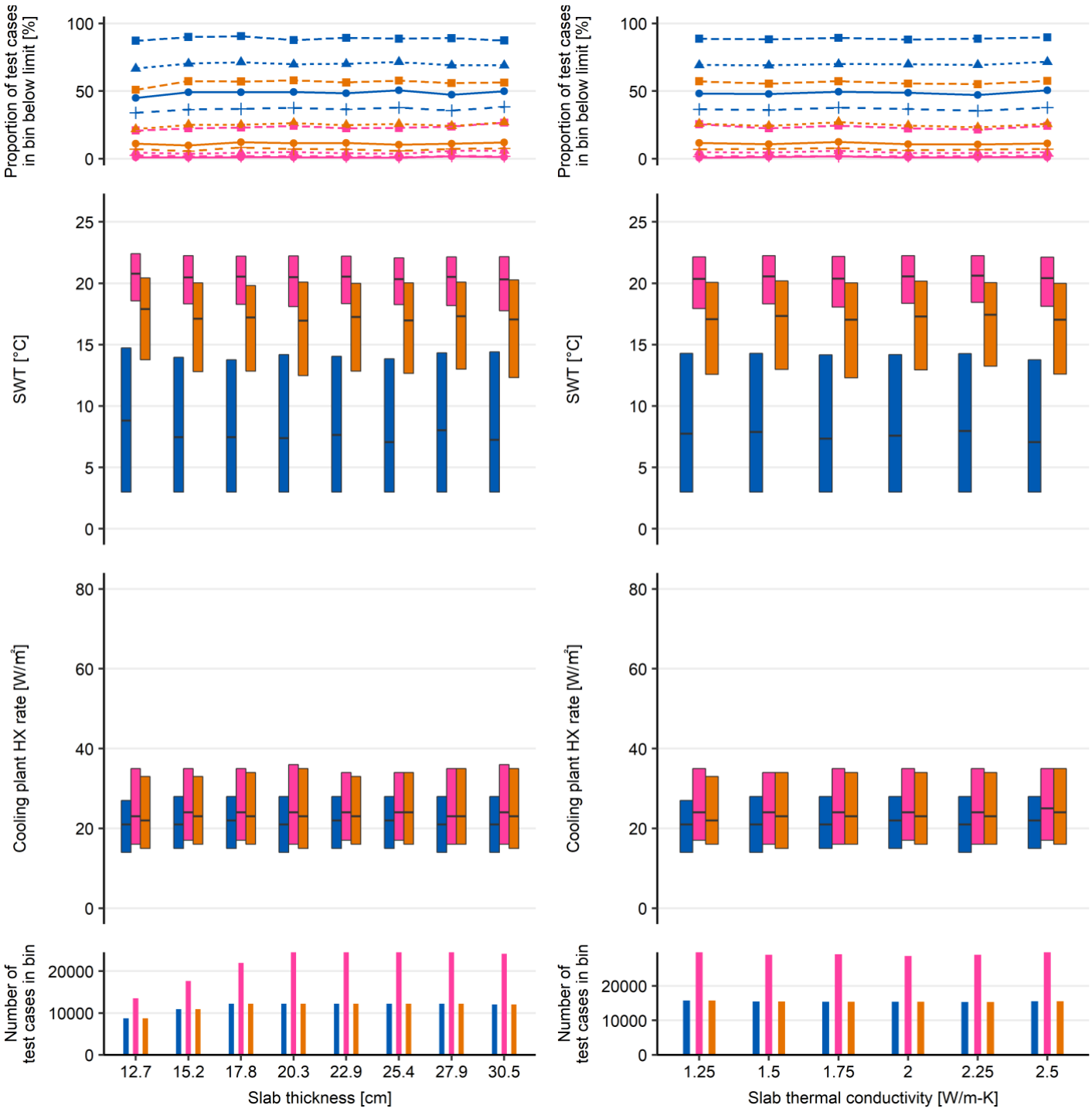

https://doi.org/10.1016/j.enbuild.2025.115387
escholarship.org/uc/item/3812p9p1

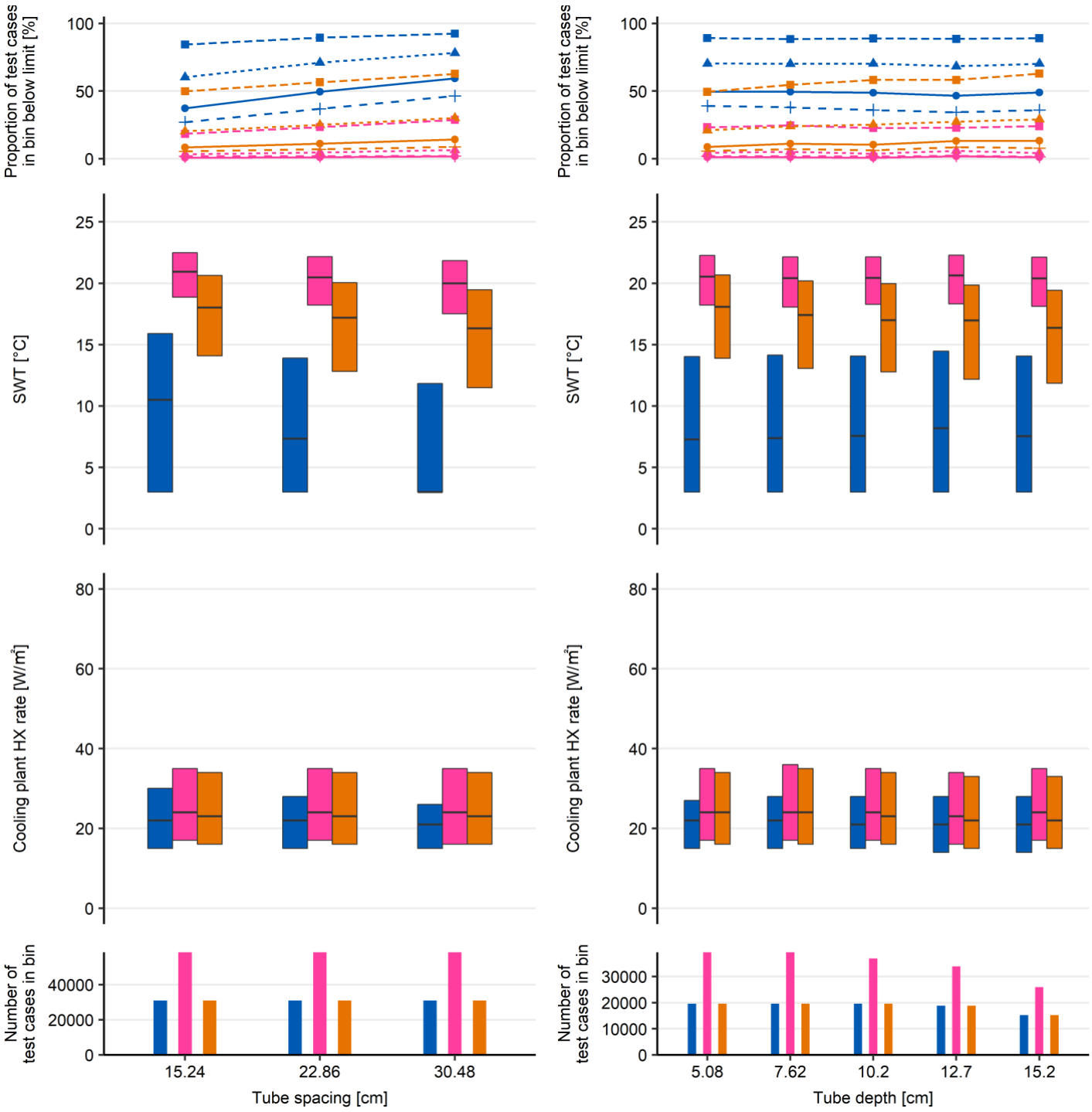

https://doi.org/10.1016/j.enbuild.2025.115387
escholarship.org/uc/item/3812p9p1

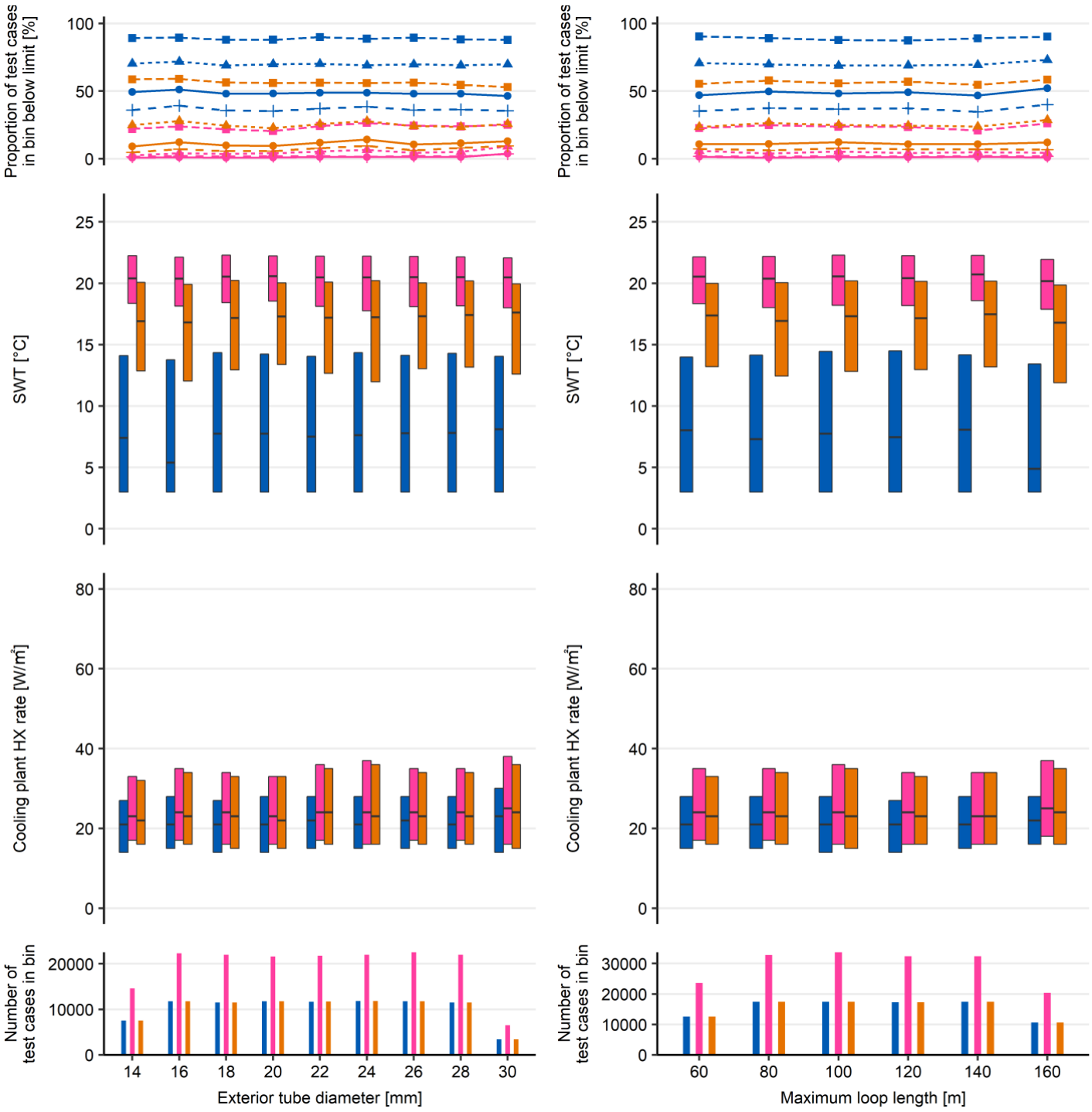

https://doi.org/10.1016/j.enbuild.2025.115387
escholarship.org/uc/item/3812p9p1

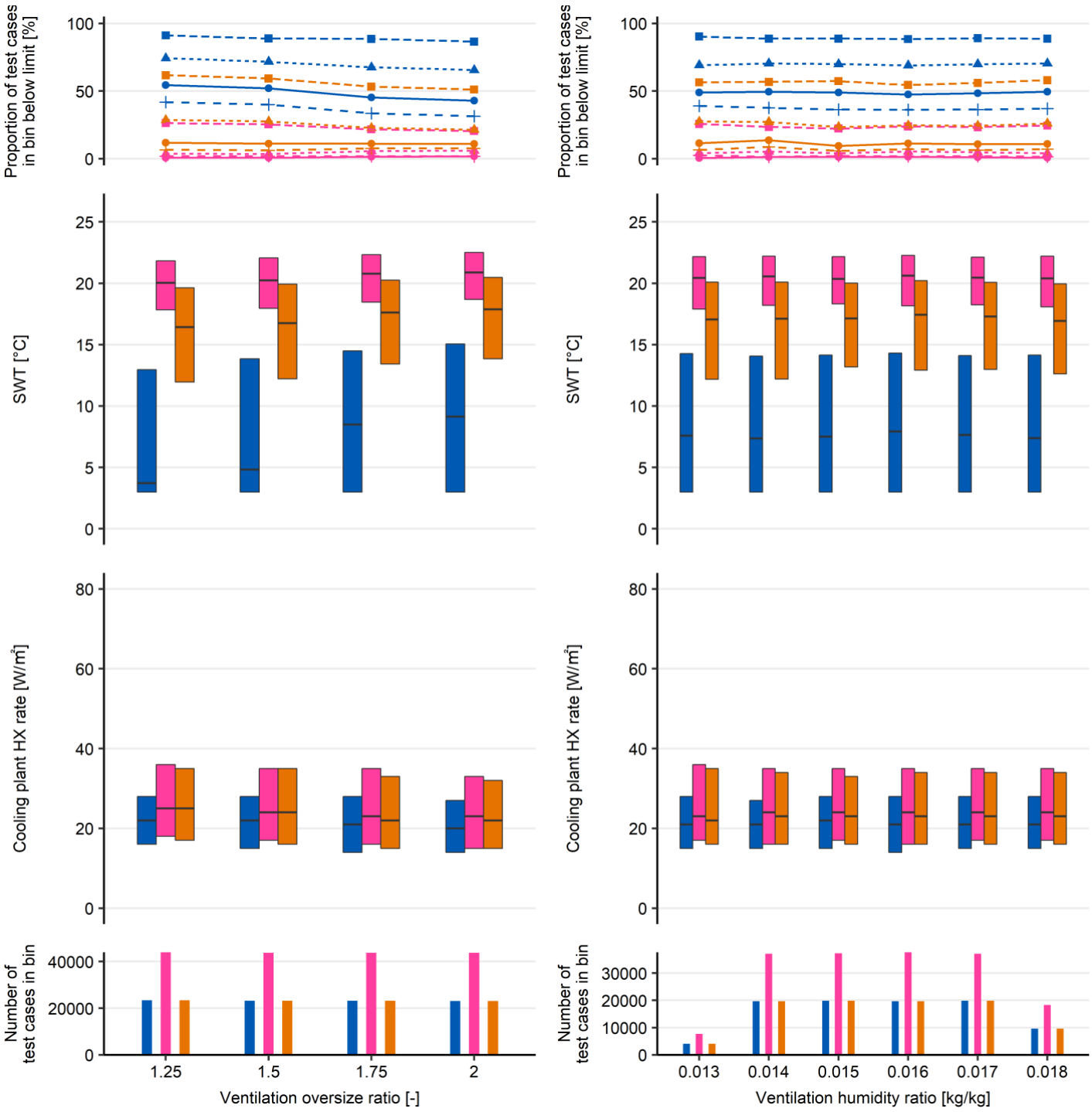

https://doi.org/10.1016/j.enbuild.2025.115387
escholarship.org/uc/item/3812p9p1

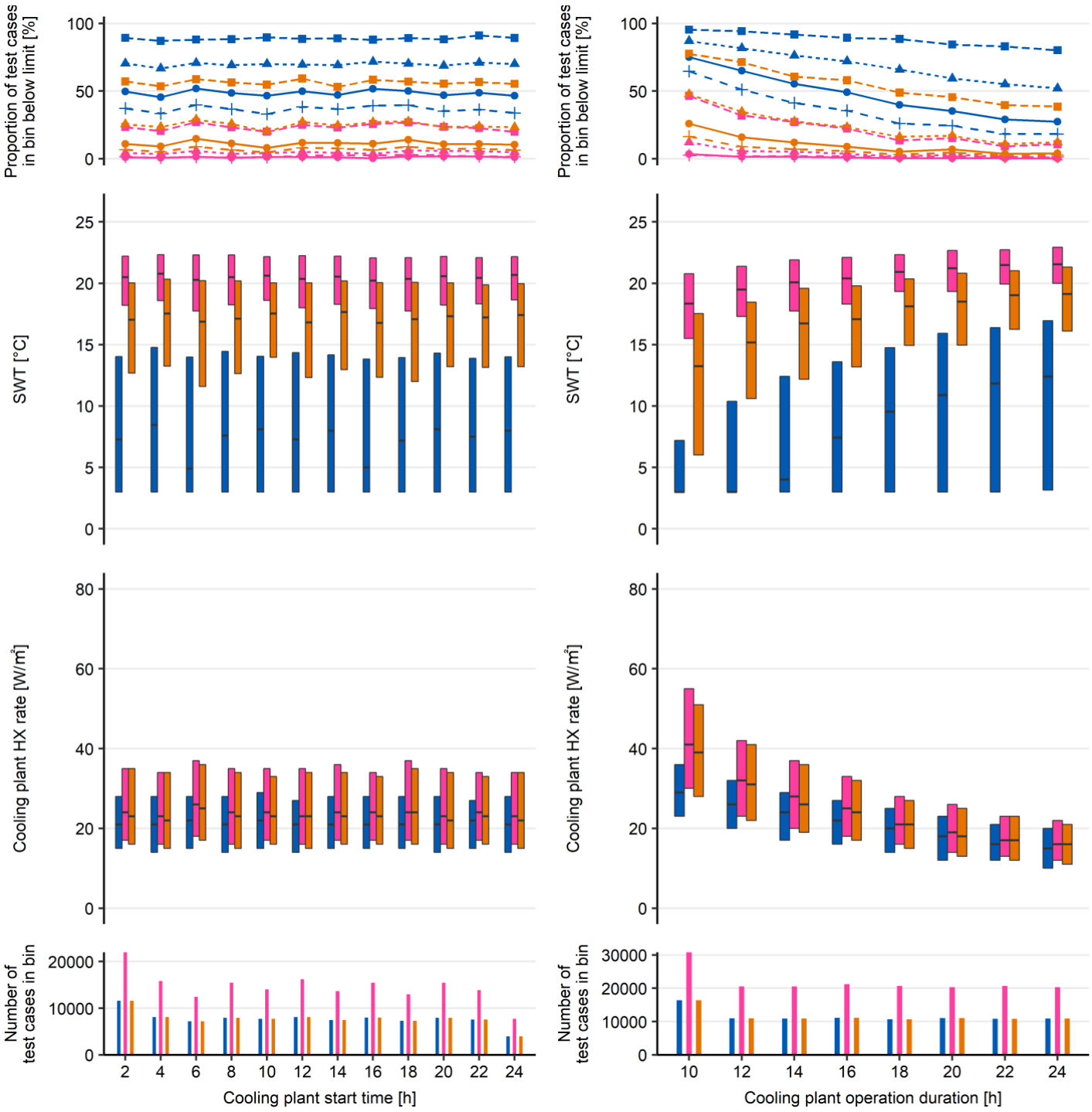

https://doi.org/10.1016/j.enbuild.2025.115387
escholarship.org/uc/item/3812p9p1

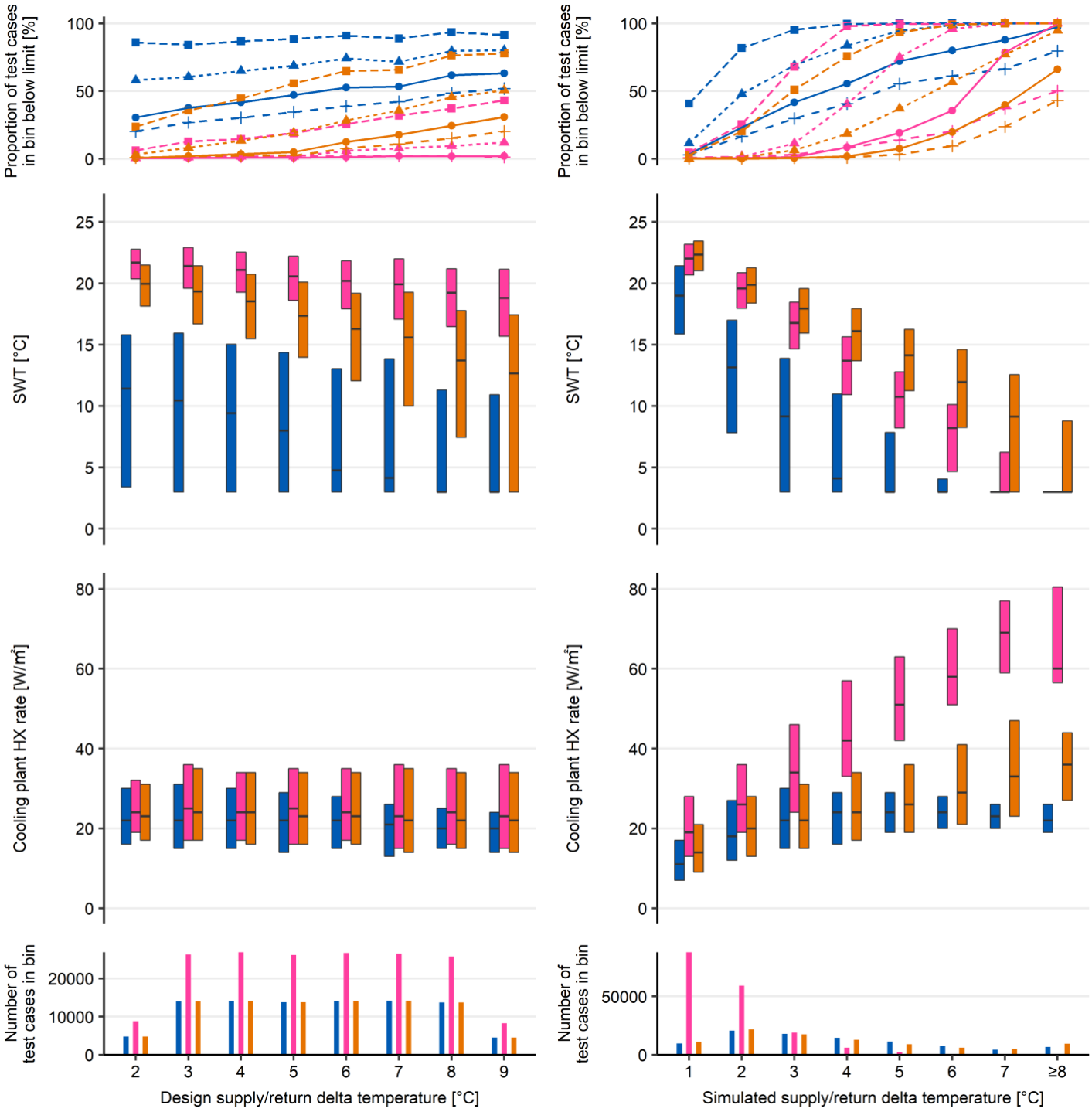

https://doi.org/10.1016/j.enbuild.2025.115387
escholarship.org/uc/item/3812p9p1

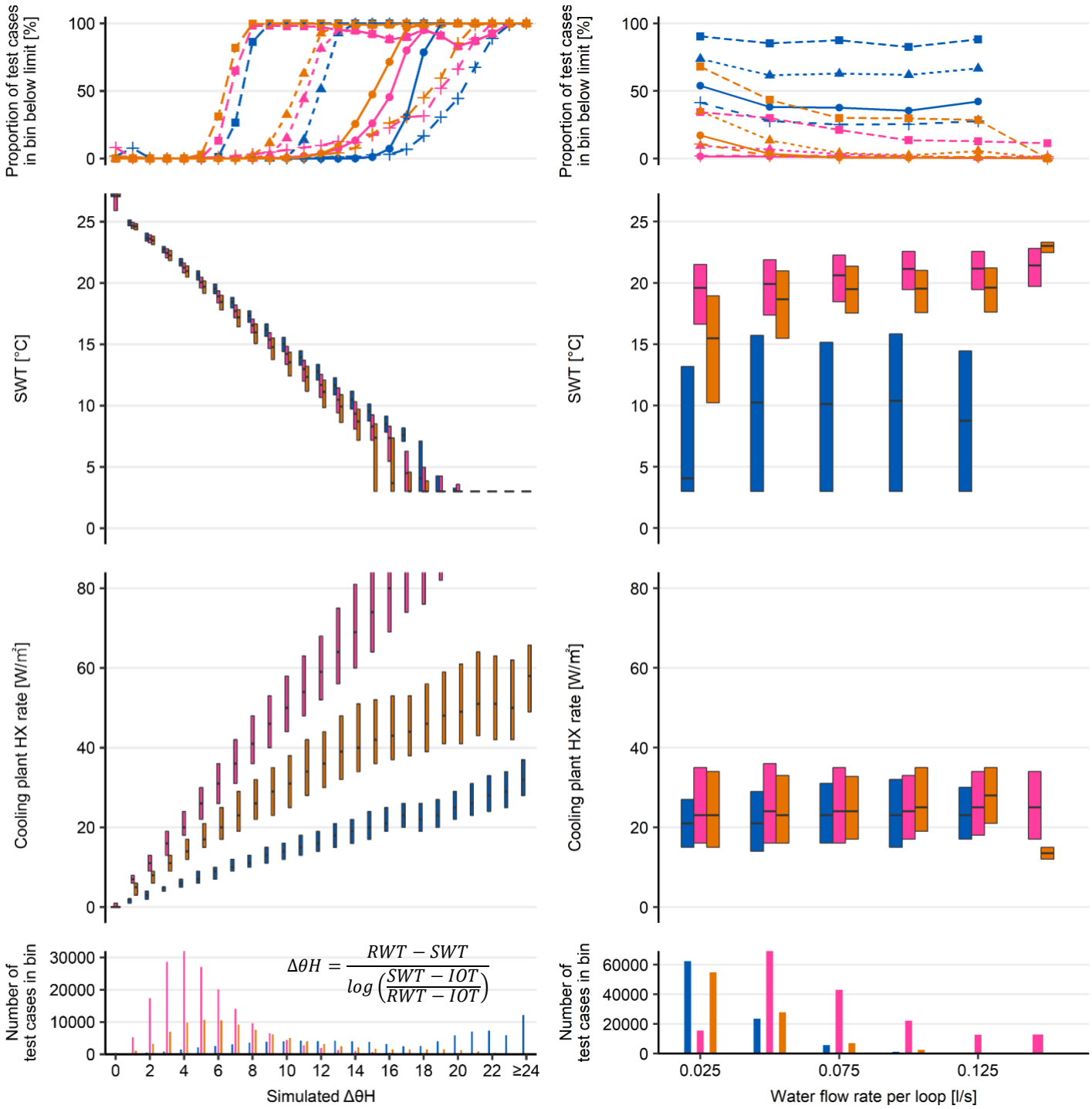

https://doi.org/10.1016/j.enbuild.2025.115387
escholarship.org/uc/item/3812p9p1

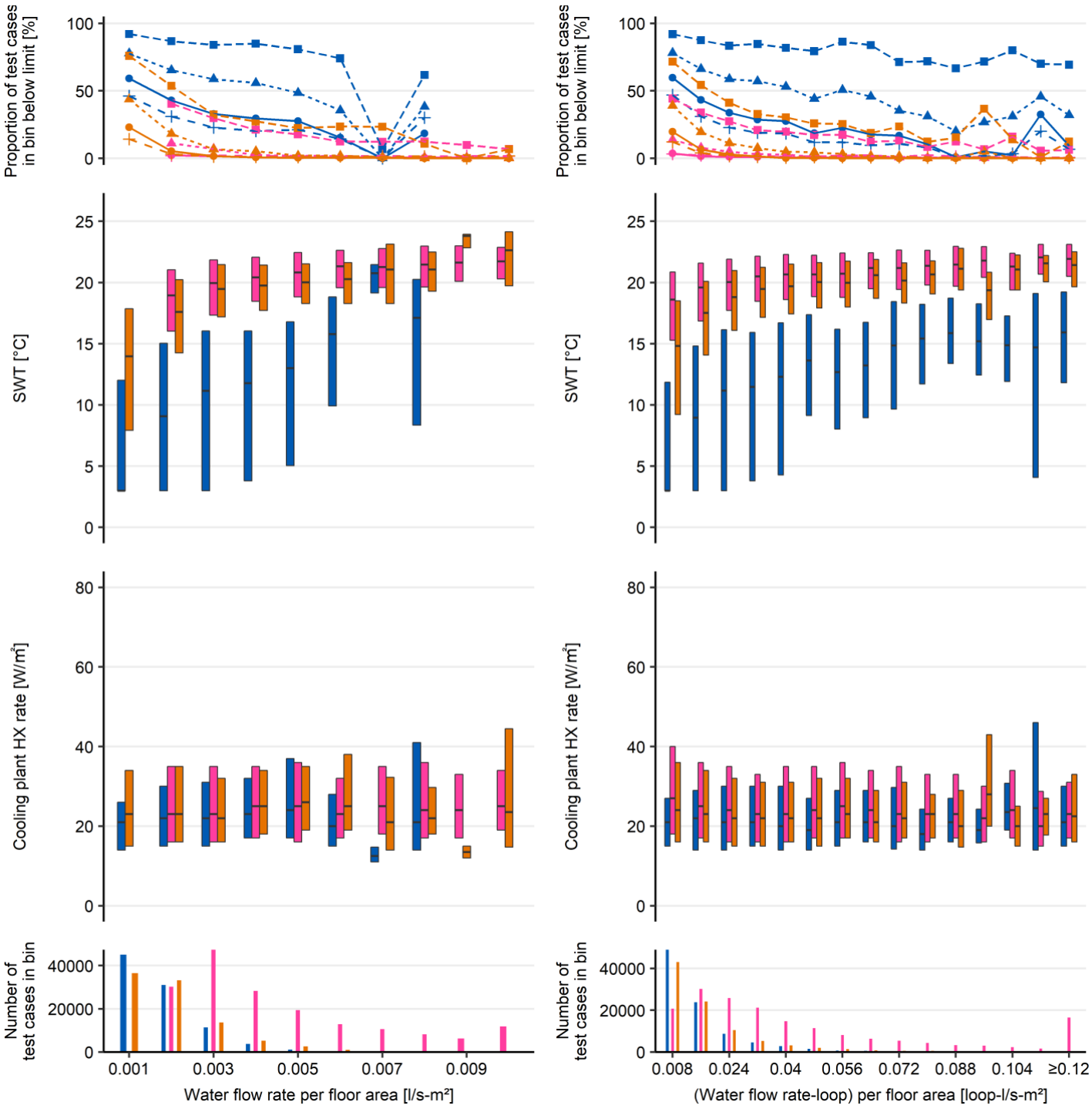

https://doi.org/10.1016/j.enbuild.2025.115387
escholarship.org/uc/item/3812p9p1

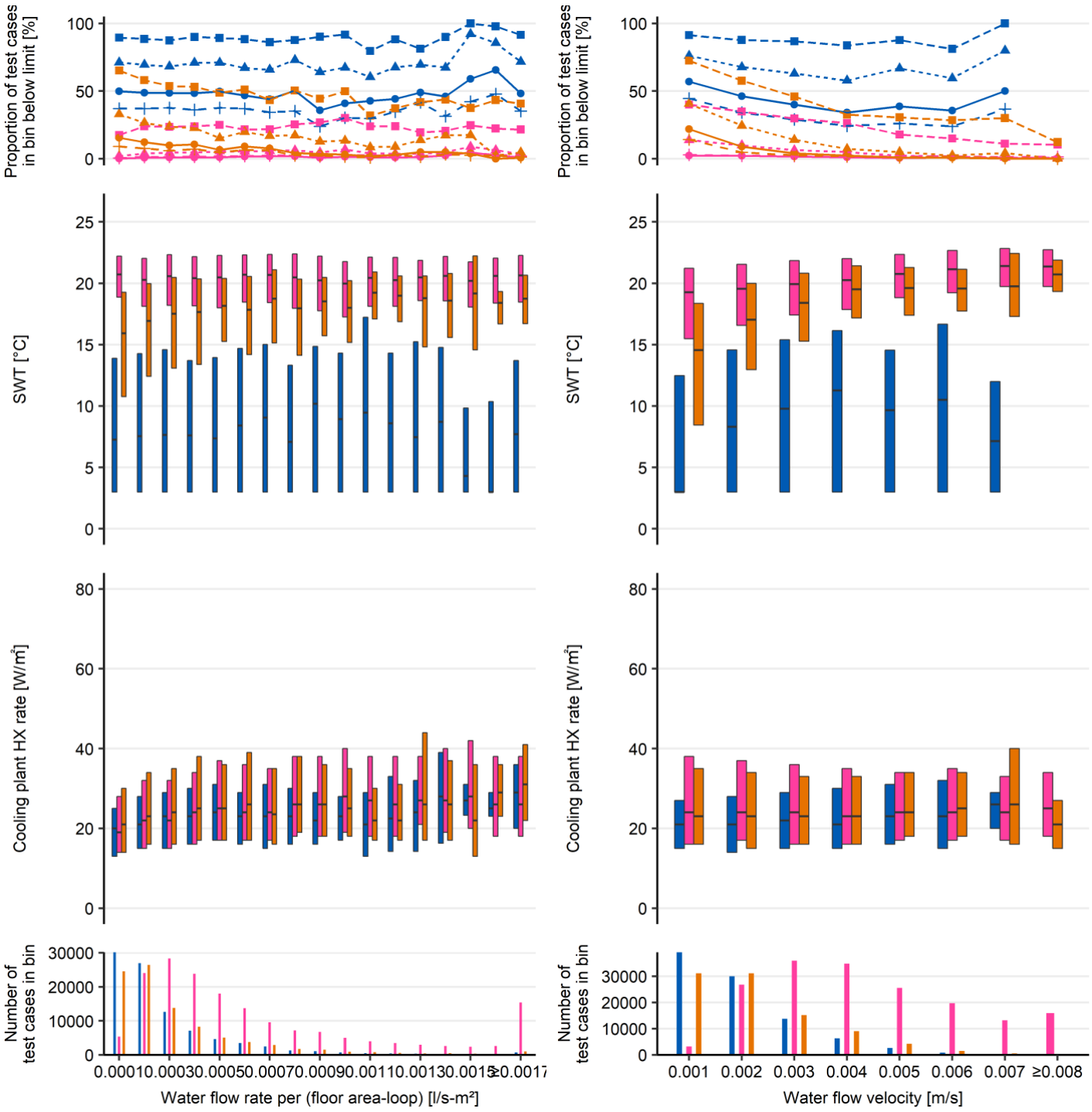

https://doi.org/10.1016/j.enbuild.2025.115387
escholarship.org/uc/item/3812p9p1

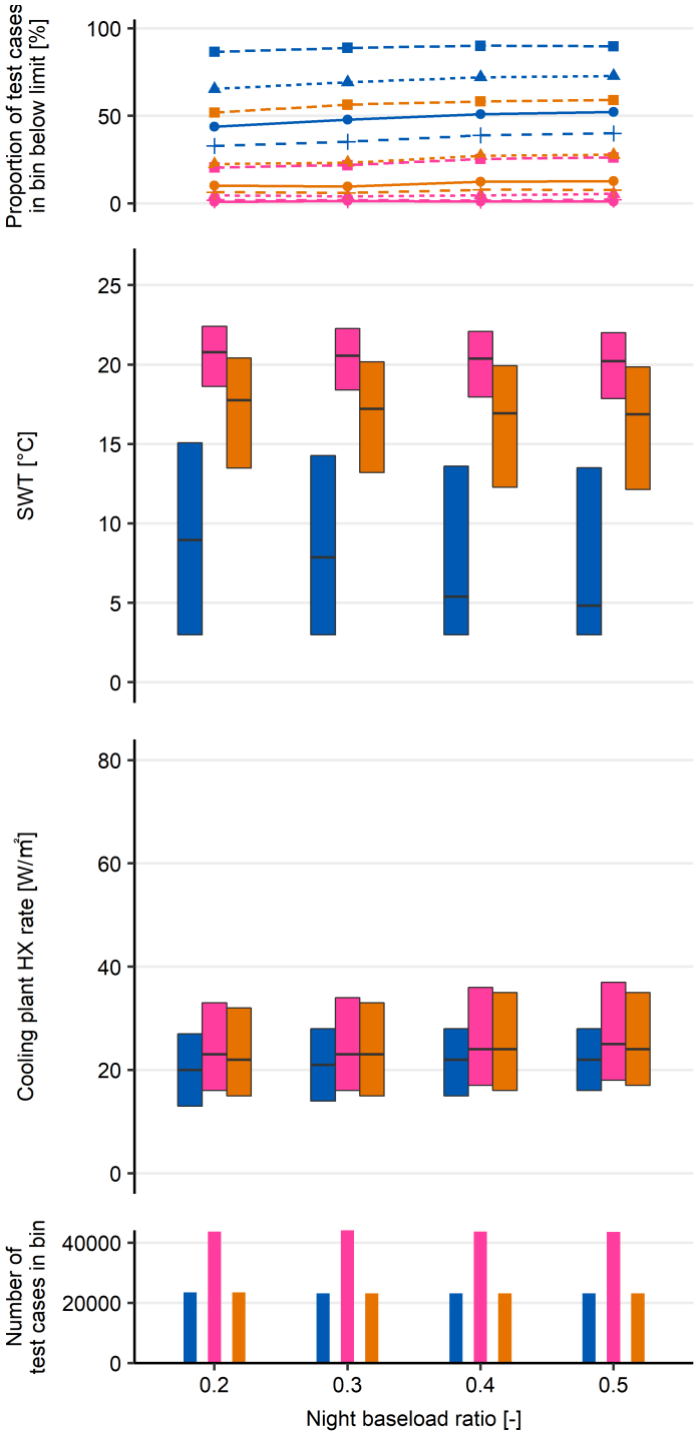

Figure c-1: The effects of various building and high thermal mass radiant design parameters on supply water temperature (SWT) and mean hydronic heat extraction (HX) rate during its operation, i.e. cooling plant HX rate. Any gray dashed line in plot indicates where y=x.

https://doi.org/10.1016/j.enbuild.2025.115387
escholarship.org/uc/item/3812p9p1